frontiers | Frontiers in Ecology and Evolution

HYPOTHESIS AND THEORY
published: 07 July 2022
doi: 10.3389/fevo.2022.903795

Human Occupation of the North American Colorado Plateau ~37,000 Years Ago

Timothy B. Rowe[1,2], Thomas W. Stafford Jr.[3], Daniel C. Fisher[4], Jan J. Enghild[5], J. Michael Quigg[6†], Richard A. Ketcham[1], J. Chris Sagebiel[2], Romy Hanna[1] and Matthew W. Colbert[1]*

[1] High-Resolution X-Ray Computed Tomography Facility, Jackson School of Geosciences, University of Texas at Austin, Austin, TX, United States, [2] Vertebrate Paleontology Laboratory, Jackson School of Geosciences, University of Texas at Austin, Austin, TX, United States, [3] Stafford Research, LLC, Albuquerque, NM, United States, [4] Museum of Paleontology, Department of Earth and Environmental Sciences and Department of Ecology and Evolutionary Biology, University of Michigan, Ann Arbor, MI, United States, [5] Laboratory for Proteome Analysis and Protein Characterization, Department of Molecular Biology and Genetics, Aarhus University, Aarhus, Denmark, [6] The Gault School of Archaeological Research, University of Texas at Austin, Austin, TX, United States

Calibrating human population dispersals across Earth's surface is fundamental to assessing rates and timing of anthropogenic impacts and distinguishing ecological phenomena influenced by humans from those that were not. Here, we describe the Hartley mammoth locality, which dates to 38,900–36,250 cal BP by AMS ^{14}C analysis of hydroxyproline from bone collagen. We accept the standard view that elaborate stone technology of the Eurasian Upper Paleolithic was introduced into the Americas by arrival of the Native American clade ~16,000 cal BP. It follows that if older cultural sites exist in the Americas, they might only be diagnosed using nuanced taphonomic approaches. We employed computed tomography (CT and μCT) and other state-of-the-art methods that had not previously been applied to investigating ancient American sites. This revealed multiple lines of taphonomic evidence suggesting that two mammoths were butchered using expedient lithic and bone technology, along with evidence diagnostic of controlled (domestic) fire. That this may be an ancient cultural site is corroborated by independent genetic evidence of two founding populations for humans in the Americas, which has already raised the possibility of a dispersal into the Americas by people of East Asian ancestry that preceded the Native American clade by millennia. The Hartley mammoth locality thus provides a new deep point of chronologic reference for occupation of the Americas and the attainment by humans of a near-global distribution.

Keywords: mammoth, butchery, taphonomy, pyrogenic residues, tomography, human dispersal

OPEN ACCESS

Edited by:
Anderson Santos,
Rio de Janeiro State University, Brazil

Reviewed by:
Vladimir V. Pitulko,
Institute for the History of Material Culture (RAS), Russia
Mario Dantas,
Universidade Federal da Bahia, Brazil

***Correspondence:**
Timothy B. Rowe
rowe@utexas.edu

† Deceased

Specialty section:
This article was submitted to Paleontology, a section of the journal Frontiers in Ecology and Evolution

Received: *24 March 2022*
Accepted: *17 May 2022*
Published: *07 July 2022*

Citation:
Rowe TB, Stafford TW Jr, Fisher DC, Enghild JJ, Quigg JM, Ketcham RA, Sagebiel JC, Hanna R and Colbert MW (2022) Human Occupation of the North American Colorado Plateau ~37,000 Years Ago. Front. Ecol. Evol. 10:903795. doi: 10.3389/fevo.2022.903795

INTRODUCTION

Recognizing early human occupation sites in the Americas traditionally rests on discovery of *in situ*, elaborately worked stone tools (Meltzer, 2009, 2015). The origins of this technology trace back to the 'Upper Paleolithic revolution' in Western Europe ~45,000 years ago (Bar-Yosef, 2002). Elaborate, stylized stone tools then spread from Western Europe into central Asia and Siberia and were later introduced into the Americas by ancestors of the Native American clade ~16,000 cal BP (Meltzer, 2009; Waters, 2019). The oldest evidence of Upper Paleolithic stone technology in the Americas is

generally equated with arrival of the first humans. However, genomic evidence for two founding populations in the Americas raises the possibility of two separate human dispersals, the first preceding arrival of Native Americans by millennia (Raghavan et al., 2014; Skoglund et al., 2015; Reich, 2018). If true, the first arrival of humans was an event entirely separate from the introduction of Upper Paleolithic technology into the Americas. If humans who lacked elaborate stone tools occupied the Americas long before arrival of the Native American clade, how might we diagnose these older occupations in the archeological record?

The Hartley locality is an open-air site on the Colorado Plateau in northern New Mexico, perched 1970 meters (m) above mean sea level on a slump block high on the wall of Rio Puerco canyon (**Figures 1**, **2**). It was discovered by Mr. Gary Hartley, who was hiking a game trail connecting the high grassy plain of La Joya del Pedrigal to riparian habitat along Rio Puerco, ∼90 m below (**Supplementary Figure 1**). A tusk was visible eroding through the surface of a wedge of colluvial sediments filling a narrow catchment trough along the top of the slump block. The tusk pointed toward three ribs and a broken dentary also eroding through the colluvial surface. A heavily reworked obsidian Clovis projectile point, and scattered lithic debitage of Pedernal chert and obsidian were exposed on the surface within a few meters of the tusk. Preliminary excavation indicated more bones were buried in the sediment wedge.

In situ associations between diagnostic Clovis projectile points and mammoths are well-known (Frison and Todd, 1986; Waters and Stafford, 2007; Hannus, 2018), and the Hartley locality initially presented itself as a possible Clovis butchery site (Huckell et al., 2016). However, surface accumulations can be mixed and time-averaged (Kowalewski et al., 1998), so the lithic accumulation might not be coeval with the buried mammoth bones. To test the association and investigate site formation processes, two seasons of hand excavation (∼7 m^3) focused on the region between and below the exposed tusk and ribs. This revealed disarticulated, intermingled partial skeletons of a young-adult female mammoth (**Figure 3**) and a young calf (**Supplementary Figure 2**), mostly piled in a meter-thick concentration of broken bones and fist-sized cobbles, with the adult face and tusks stacked on top (**Supplementary Information**).

The more obvious features of the bone assemblage suggested this was a butchery site. However, six AMS ^{14}C dates on the adult mammoth bone collagen yielded ages ranging from 38,900 to 32,300 cal BP (**Table 1** and **Figures 4**, **5**). These dates are far too old to be cultural according to prevailing archeological views (e.g., Meltzer, 2009; Waters, 2019). However, they lie within the time range hypothesized by genomic evidence, which projects a human presence in the Americas as early as 56,000 years ago (Wohns et al., 2022). The dates also suggest the lithic debris on the colluvial surface was most likely a time-averaged assemblage that accumulated long after the mammoth bones were broken and buried, leaving open the question of whether the mammoth bones reflected cultural activity. The only lithic evidence recovered from excavating the Hartley site consisted of six chert microflakes found in lower levels of the excavation. Although they preserve evidence of percussion flaking (below), taphonomic analysis of the bone assemblage and surrounding sediments soon became the primary basis for elucidating site formation.

We used established techniques (Shipman, 1981; Behrensmeyer and Hill, 1988; Haynes et al., 2020), plus state-of-the-art methods that had not previously been applied to investigating ancient American sites. These include high-resolution computed tomography (HRXCT and μCT) (Carlson et al., 2003; Rowe and Frank, 2011; Frank et al., 2021), proteomic analysis of the mammoth bone collagen, environmental scanning electron microscopy (ESEM), and petrographic analysis of microparticles from the matrix. These new methods significantly expanded the range of criteria for site interpretation. Our analyses revealed diagnostic evidence of diverse human activities including systematic, highly patterned bone breakage and secondary bone flake production, pyrogenic residues indicative of a controlled (domestic) fire, and utilization of regional vertebrate microfauna. The independent lines of evidence described below support recognition of this as a cultural site.

METHODS

AMS ^{14}C Measurements on Hartley Mammoth Bone

Bones and teeth with unique scientific importance should be dated not only multiple times, but should have direct ^{14}C measured on different chemical fractions to assess how chemical purification removes exogenous contaminants (Stafford et al., 1991; Stafford, 2014; Waters et al., 2014). The specimen selected was TMM 47004-1.40 (Stafford Research [SR] sample no. 9067), a thick adult cortical bone fragment that we identified as a butterfly fragment (below), from either an ulna or tibia (**Figure 6F**). The bone was dateable because it was moderately well preserved chemically (**Tables 1**, **2** and **Figures 4**, **5**); it yielded 2.6wt% of collagen, compared to 23wt% for modern bone (Schwarcz and Nahal, 2021). The sample also contained 0.4wt% nitrogen, compared to 4.5wt% in modern bone (Schwarcz and Nahal, 2021). The molecular weights of collagen fragments were in the >10 kDa range, with minimum and maximum values being 20 and 50 kDa, respectively. Dates were calibrated using OxCal 4.4, IntCal 20, Interface Build 133, Updated 24/11/2021, and calibrated at 2-sigma, 95.4%, and 3-sigma 99.7% probabilities (Reimer, 2020).

Author TWS coordinated AMS ^{14}C dating of the Hartley mammoth bone to determine the age of the mammoth remains. With exceptions as noted, TWS performed chemical purifications by combusting pretreated samples to carbon dioxide (CO_2) and submitting 6 mm (outer diameter) fused quartz tubes of CO_2 for graphitization and ^{14}C measurement using three different AMS ^{14}C facilities. One sample was sent to the University of Georgia Accelerator Mass Spectrometer Radiocarbon Dating Laboratory (UGAMS), and two samples were processed at the University of California, Irvine, Accelerator Mass Spectrometer (UCIAMS). TWS also sent subsamples of SR-9067 to the Oxford Radiocarbon

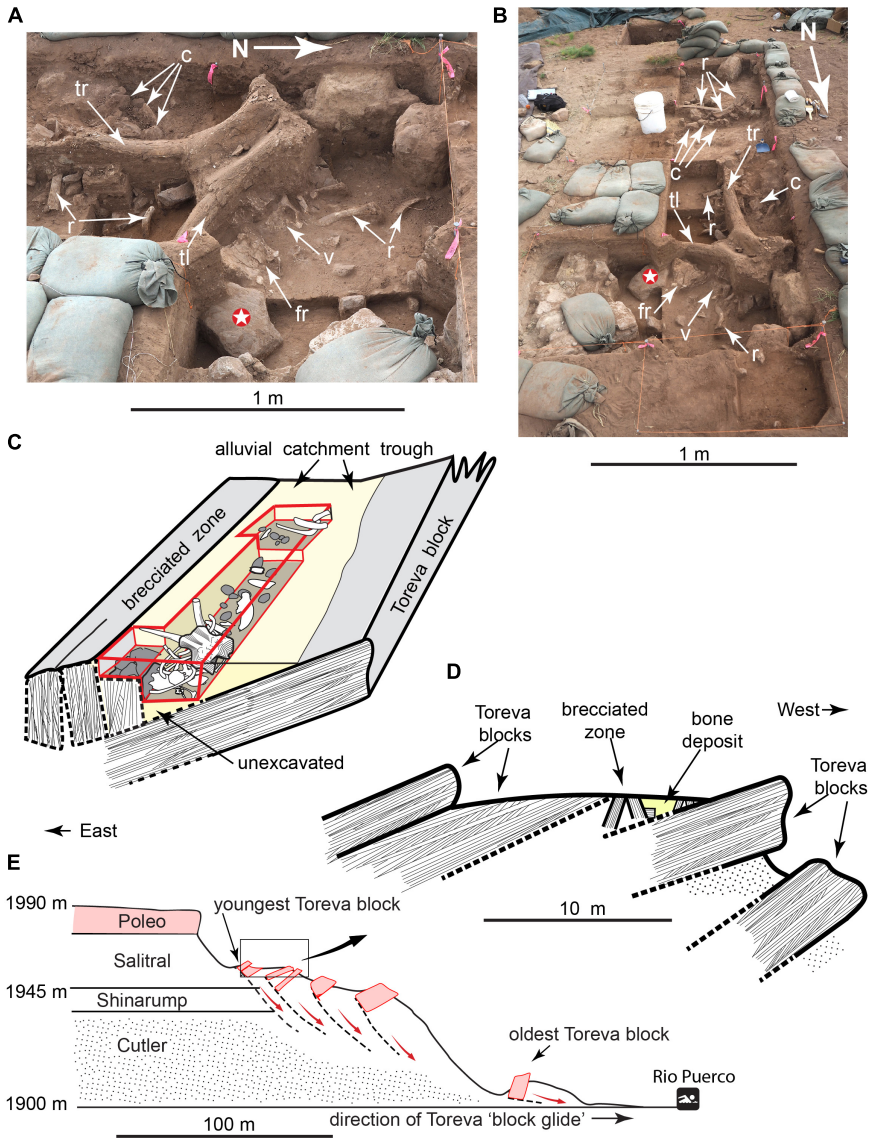

FIGURE 1 | Hartley mammoth excavation. **(A,B)** Uppermost part of main bone accumulation. **(C)** Diagram of bone-bearing sediment wedge (not to scale). **(D)** Schematic of Toreva block landslides. **(E)** Cross-section of Rio Puerco canyon. C, sandstone cobbles; R, rib; Tl, left tusk; Tr, right tusk; Fr, frontal; V, thoracic vertebra; white star, 23.7 kg hammerstone/anvil.

Unit (ORAU; University of Oxford) for processing and dating by Dr. Lorena Becerra-Valdivia (OxA, below).

Our initial exploratory ^{14}C measurement was on 0.45 μm-filtered gelatin from potassium hydroxide (KOH)-extracted collagen, and it yielded an age of 28,745 ± 86 RCYBP (UGAMS-A24643), equivalent to 33,700 – 32,300 cal BP. Extensive ^{14}C and stable isotope analyses on the mammoth bone then followed.

A second ^{14}C date was obtained using methods for chemical purification of bone collagen described by Stafford (2014) and Devièse et al. (2017, 2018a,b). Bone was crushed into ∼2–4 mm fragments and decalcified in 0.6M hydrochloric acid (HCl) at 4°C, washed with deionized (DI) water, extracted over 24 h with 0.01M KOH at 4°C, washed to neutrality, acidified with 0.05M HCl and the alkali-extracted collagen freeze-dried and weighed to obtain a weight percent yield relative to 23wt% for modern bone. Next, 20–25 mg of lyophilized collagen were heated in 0.05M HCl at 90°C until dissolution was complete, ∼20–30 min. The solution (gelatinized collagen) was passed through a 0.45 μm Millipore filter and freeze-dried. Finally, 15–20 mg of dry gelatin were heated at 110°C for 24 h in sealed Pyrex tubes to hydrolyze the gelatin to free amino acids. This hydrolyzate was passed through a column containing 1 cc of Restek XAD-2 resin, the eluate filtered through a 0.45 μm Millipore membrane and the XAD-purified hydrolyzate dried over a N_2 stream at 40°C. Subsamples collected from each step were used for amino acid, $\delta^{13}C$, $\delta^{15}N$, and ^{14}C analysis. The sample was graphitized at the

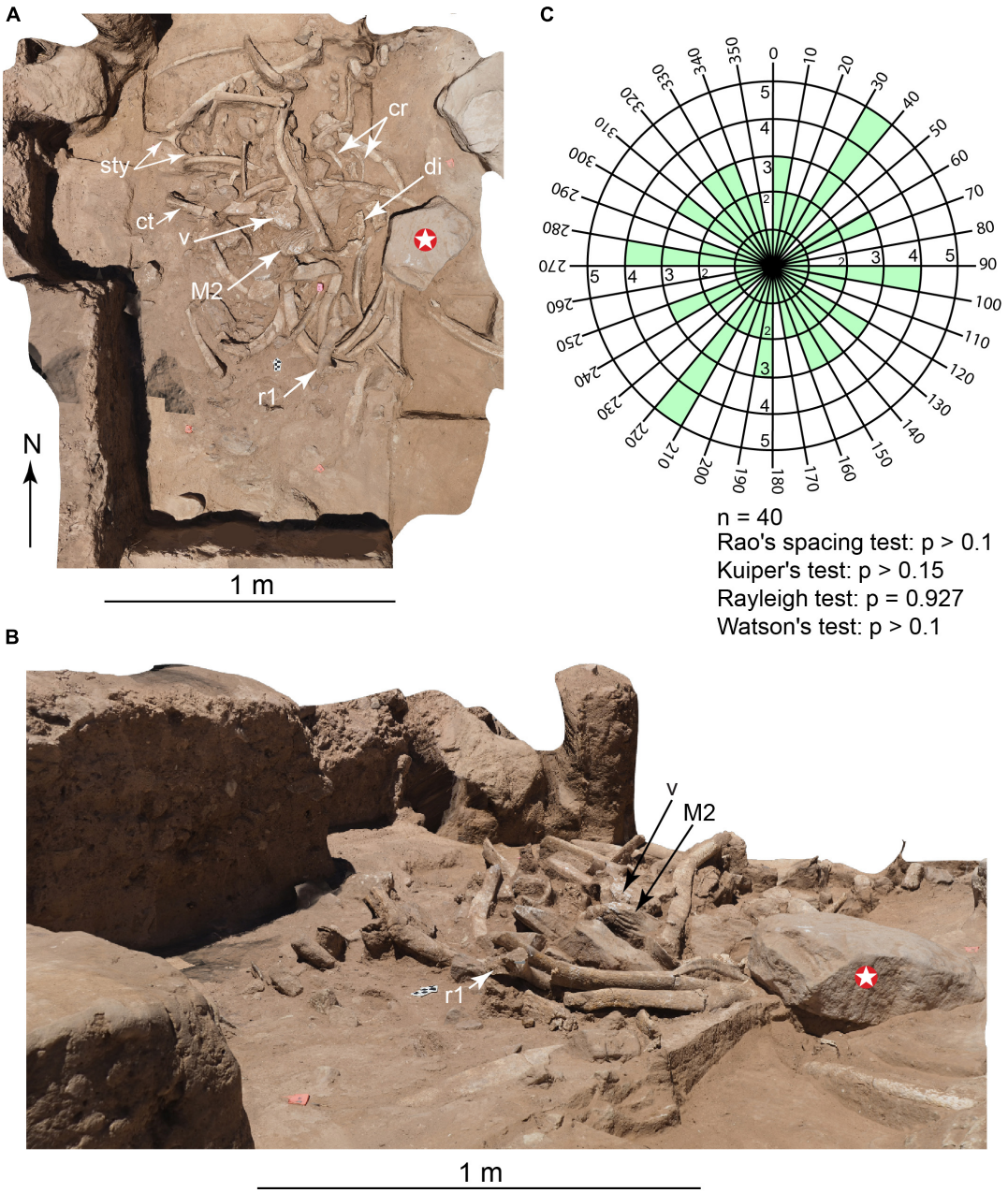

FIGURE 2 | Main bone accumulation, following removal of adult face. (Photogrammetry images). **(A)** Overhead view. **(B)** Oblique view. **(C)** Bi-directional rose diagram showing random orientation of 40 elongate elements exposed; see text for explanation. Cr, calf ribs; Ct, calf tibia; Di, adult cranial diplöe; M2, adult upper second molar; R1, adult first rib; V, adult thoracic vertebra; Sty, adult stylohyoid; white star, 23.7 kg hammerstone/anvil.

UC Irvine AMS facility, and the resulting date on the XAD-2 purified fraction was 30,860 ± 220 RCYBP (UCIAMS-205817), equivalent to 35,750 – 34,600 cal BP.

A third date on ultrafiltered (>30 kDa) gelatin was processed at the UC-Irvine AMS facility using protocols described online in the following document: https://sites.uci.edu/keckams/files/2016/12/bone_protocol.pdf. It produced a measurement of 28,360 ± 230 RCYBP (UCIAMS-191867), equivalent to 33,250 – 31,750 cal BP.

Finally, a series of three dates on subsamples of SR-9067 were processed by Dr. Lorena Becerra-Valdivia at the Oxford AMS facility and included ages on 60–90 μm-filtered gelatin, ultrafiltered gelatin and the individual amino acid, hydroxyproline, using protocols described in Hedges and van Klinken (1992) and Devièse et al. (2017, 2018a,b). The first sample used pretreatment code (P-code) 'AG,' which is a routine procedure involving decalcification, base wash, reacidification, gelatinization, and filtration of bone using previously cleaned

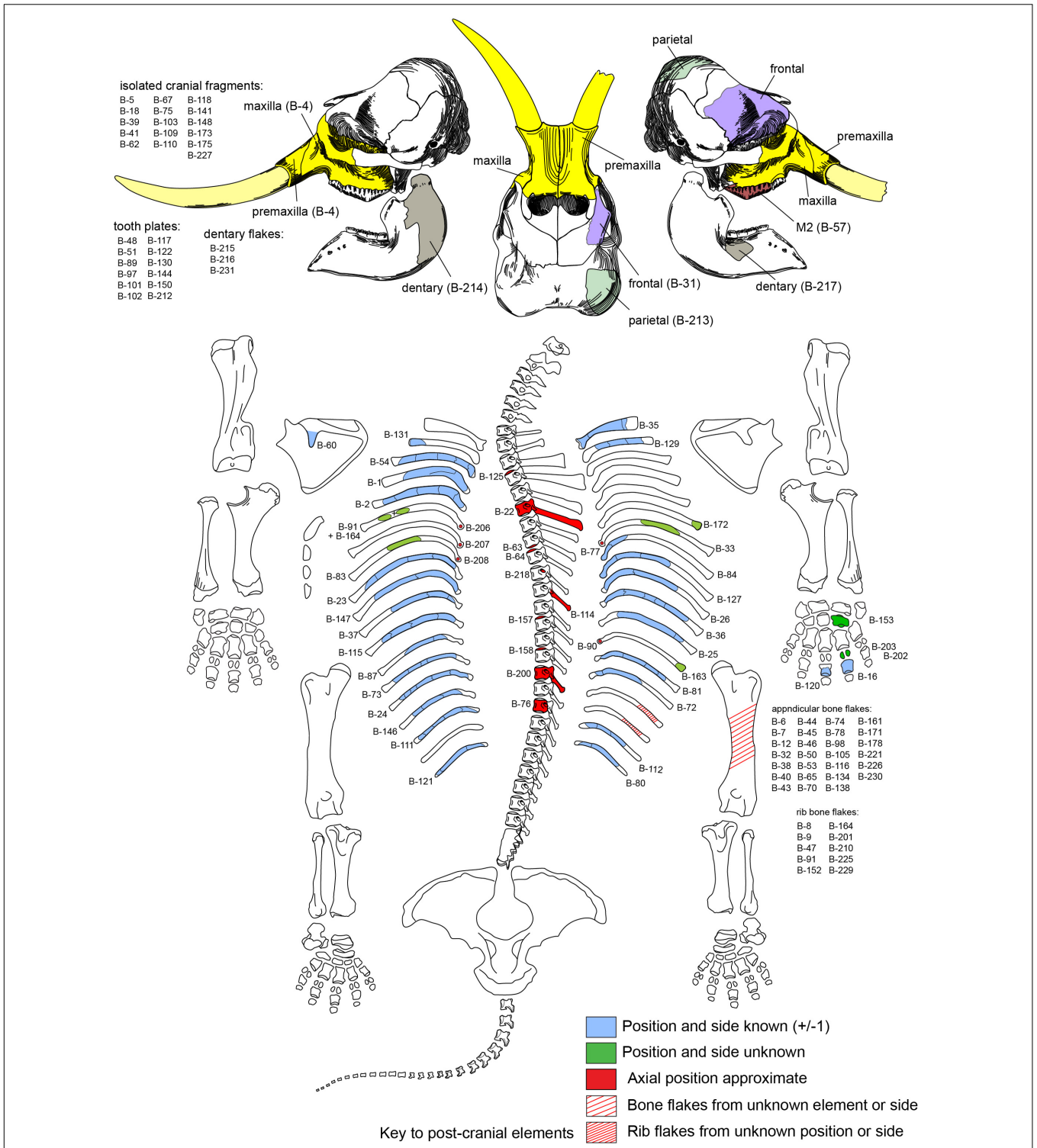

FIGURE 3 | Recovered parts of adult mammoth. Numbers refer to cataloged bones with the prefix TMM 47004-1.X.

9 ml Ezee-filters (Elkay, United Kingdom), following Brock et al. (2010). The result was 28,100 ± 350 RCYBP (OxA-36306), equivalent to 33,250 – 31,300 cal BP.

The second P-code, 'AF,' is another routine protocol that includes ultrafiltration (using Vivaspin 15–30 kDa MWCO) of the gelatin following Ezee filtration as described by

Brock et al. (2010). The result obtained is 29,520 ± 340 RCYBP (OxA-36,358), equivalent to 34,650 – 33,200 cal BP.

The last protocol, P-code 'NRC' (non-routine chemistry), involves separation of underivatized amino acids from ultrafiltered, hydrolyzed collagen and isolation of hydroxyproline using a preparative High Performance Liquid Chromatography (prep-HPLC) approach. A full description of this protocol, optimized at the ORAU, can be found in Devièse et al. (2017, 2018a,b). Collected collagen and hydroxyproline samples were dried, combusted, graphitized, and AMS-dated as described by Brock et al. (2010), and with HPLC carbon contribution corrections made per Devièse et al. (2018b). The result is 32,750 ± 430 RCYBP (OxA-X-2737-56), equivalent to 38,900 – 36,250 cal BP. These results show that the first five dates are in good agreement with each other, while the hydroxyproline measurement is older. Considering the NRC protocol to be more efficient than the other protocols for removing exogenous carbon from bone (collagen) samples (Rappsilber et al., 2007; He et al., 2015), the latter date (32,750 ± 430 RCYBP, equivalent to 38,900 – 36,250 cal BP), is considered the most robust age estimate for sample SR-9067.

Amino Acid and Liquid Chromatography-Tandem Mass Spectrometry Proteomic Analyses

To assess quantitatively the preservation and composition of the collagen isolated for AMS radiocarbon dating, JJE performed quantitative amino acid and liquid chromatography-mass spectrometry/mass spectrometry (LC–MS/MS) analyses on the adult mammoth bone, SR-9067 (**Table 2**). Amino acids were measured using the Biochrom 30+ high-performance liquid chromatography cation exchange system with ninhydrin detection. While atomic C/N values are commonly used to certify preservation quality of collagen (Schwarcz and Nahal, 2021), such analyses only indicate that the decalcified bone or dentin being analyzed does not contain a preponderance of non-proteinaceous material. Collagen is identified by its unique amino acid composition, which is 9% percent (or 90 residues/1000) hydroxyproline (HYP) and 33% (or 338 residues/1000) glycine (GLY) (**Table 2**). Mammoth bone SR-9067 was decalcified with two different reagents (0.6M HCl and 0.5M EDTA), and amino acid compositions were measured for those residues (**Table 2**). The results are values for slightly degraded collagen, where HYP values have decreased from a modern value of 9% (or 90 residues/1000) to the 5% (or 49 residues/1000) present in the Hartley mammoth collagen (**Table 2**). These diagenetic changes in fossil collagen's amino acid composition are well documented (Stafford et al., 1991, Stafford, 2014) and involve proportional decreases in HPY and relative increases in aspartic and glutamic acids as overall collagen content decreases over time. All samples were desalted by micropurification using Empore SPE Disks of C18 octadecyl packed in 10 μl pipette tips. LC-MS/MS was performed using either an EASY-nLC 1000 system (Thermo Fisher Scientific, Waltham, MA, United States) connected to a Q Exactive + Hybrid Quadrupole-Orbitrap Mass Spectrometer (Thermo Fisher Scientific, Waltham, MA, United States) through a Nanospray Flex Ion Source (Thermo Fisher Scientific, Waltham, MA, United States) or an eksigent nanoLC 415 system (Sciex, Torrence, CA, United States) connected to a TripleTOF 6600 mass spectrometer (Sciex, Torrence, CA, United States) equipped with a NanoSpray III source (Sciex, Torrence, CA, United States). Peptides were dissolved in 0.1% formic acid, injected, trapped and desalted on a ReproSil-Pur C18-AQ trap column (2 cm × 100 μm inner diameter packed in-house with 3 μm resin; Dr. Marisch GmbH, Ammerbuch-Entringen, Germany). The peptides were eluted from the trap column and separated on a 15-cm analytical column (75 μm inner diameter) packed in-house in a pulled emitter with ReproSil-Pur C18-AQ 3 μm resin (Dr. Marisch GmbH, Ammerbuch-Entringen, Germany). Peptides were eluted using a flow rate of 250 nl/min and a 50 min gradient from 5 to 35% phase B (0.1% formic acid and 90% acetonitrile or 0.1% formic acid, 90% acetonitrile and 5% DMSO). The collected MS files were converted to Mascot generic format (MGF) using the SCIEX MS Data Converter beta 1.1 (Sciex, Torrence, CA, United States) or RawConverter (Stafford et al., 1991).

Computed Tomographic Scanning

All CT and μCT scanning was performed at the University of Texas High-Resolution X-ray Computed Tomography Facility (UTCT). Instrument specifications are detailed at: http://www.ctlab.geo.utexas.edu. See **Supplementary Information** for scan parameters for each specimen described in this report. CT images were processed and measurements were taken using Aviso 2019.3, VG Studio Max 2.1, and NIH Image J.

Environmental Scanning Electron Microscopy

Microparticles were mounted on SEM stubs and analyzed in backscatter mode using a Philips XL30 ESEM TMP scanning electron microscope, and a JEOL JSM6490 scanning electron microscope, using EDAX Genesis energy-dispersive X-ray analysis for elemental analysis.

SITE DESCRIPTION

Although extensively broken, the mammoth bones exhibit little evidence of weathering or hydrologic transport abrasion, and modest root etching. None of the bones exhibits tooth marks or other evidence of carnivore scavenging (**Supplementary Information**). The bones were buried by low-energy slope-wash in a colluvial matrix (**Supplementary Information**). CT and μCT revealed an anastomosing postmortem burrow in one vertebra that we interpret as termite-like insect activity. Occasional cicada burrows penetrated sediments around and inside the broken bones. Bone breakage from sediment loading is minor. We considered scavenging, trampling, and other non-anthropogenic agents in our assessment of site formation processes (**Supplementary Information**), but the likelihood is exceedingly small that these can account for the thorough, intensive, systematic and highly

TABLE 1 | AMS ^{14}C chronometric data for bone collagen from adult Hartley mammoth.

AMS lab no.	Sample no.	Taxon	*Skeletal element*	Sample ID	Chemical fraction dated	Fraction modern (Fm)	Fm ± 1 SD	δ^{15}N ‰ (AIR)	δ^{13}C ‰ (VPDB)	C/N (Atomic)	^{14}C Age, RC yr. BP	± 1 SD	CALBP 2 SD (95.4%)
UGAMS-A24643	SR-9067	*Mammuthus* spp.	*Ulna or Radius diaphysis*	FN B40, N208.741 E98.122	0.45 μm-filtered Gelatin from KOH-Collagen	0.0279	0.0003	_	–19.6	_	28,745	86[1]	33,700–32,300
OxA-36306	SR-9067	*Mammuthus* spp.	*Ulna or Radius diaphysis*	FN B40, N208.741 E98.122	Ezee (60-90 μm)-Filtered Gelatin from NaOH-extracted collagen (Oxford P-Code AG)	0.0303	0.0013	8.3	–19.4	3.4	28,100	350	33,250–31,300
UCIAMS-191867	SR-9067	*Mammuthus* spp.	*Ulna or Radius diaphysis*	FN B40, N208.741 E98.122	Ultrafiltered (> 30 kDa) Gelatin	0.0293	0.0008	8.1	-19.4	3.2	28,360	230	33,250–31,750
OxA-36358	SR-9067	*Mammuthus* spp.	*Ulna or Radius diaphysis*	FN B40, N208.741 E98.122	Ultrafiltered (>30 kDa) Gelatin (Oxford P-Code AF)	0.0253	0.0011	8.5	–19.2	3.2	29,520	340	34,650–33,200
UCIAMS-205817	SR-9067	*Mammuthus* spp.	*Ulna or Radius diaphysis*	FN B40, N208.741 E98.122	XAD-Purified Gelatin hydrolyzate from KOH-extracted collagen	0.0214	0.0006	8.1	–19.4	3.2	30,860	220	35,750–34,600
OxA-X-2737-56	SR-9067	*Mammuthus* spp.	*Ulna or Radius diaphysis*	FN B40, N208.741 E98.122	Hydroxyproline (Oxford P-Code NRC)	0.0175	0.0009	5.0	–25.5	5.8	32,750	430	38,900–36,250
Backgrounds and Known-Age Bones													
UCIAMS-205822	SR-8136	*Eschrichtius robustus* (Gray Whale)	*Rib*	Beaufort Whale, Alaska	XAD-Gelatin	0.0016	0.0001	14.0	–14.3	3.2	51,680	260	Out of Range
UCIAMS-205819	SR-9071	*Alces alces* Eurasian Elk	*Rib*	Miesenheim IV, Germany	XAD-Gelatin	0.2541	0.0007	2.5	–20.2	3.2	11,005	25	13,100–12,800

See section "Methods" for explanation of P-Codes. Calibrations made using OxCal 4.4 (11/14/2021) IntCal 20. UGAMS, University of Georgia; UCIAMS, University of California-Irvine; OxA, Oxford University. Fn, Field number (with excavation coordinates).

[1]We suspect this standard deviation is too narrow.

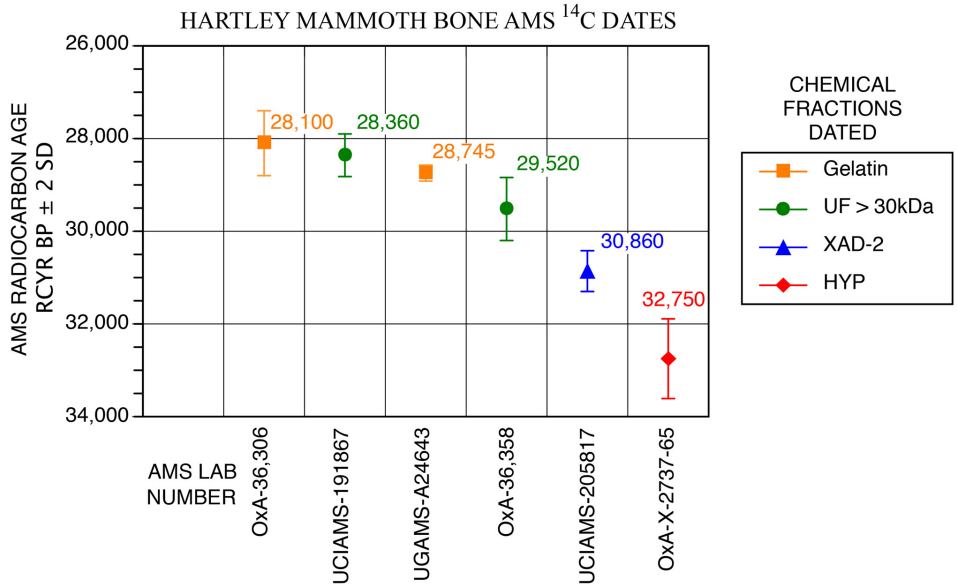

FIGURE 4 | AMS ^{14}C measurements on different Hartley mammoth bone collagen chemical fractions.

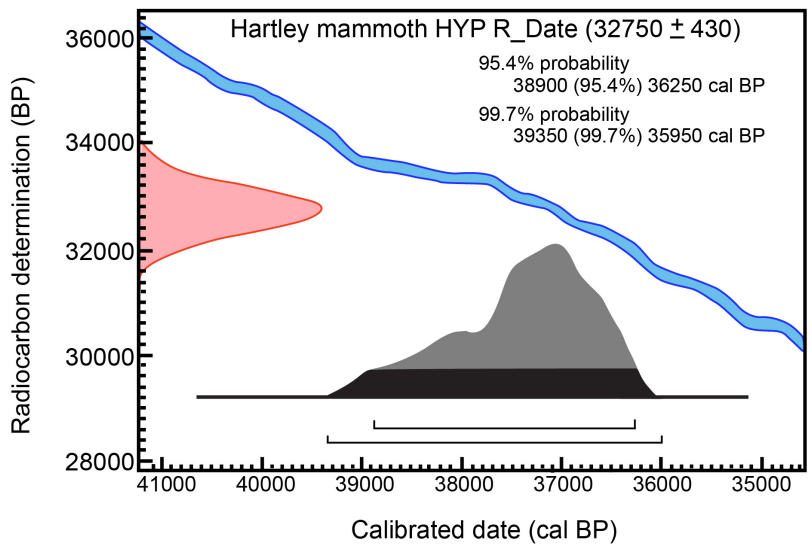

FIGURE 5 | Calibration of ^{14}C measurement on hydroxyproline from Hartley mammoth bone collagen: 32,750 ± 430 RC yr BP (OxA-X-2737-65) OxCal v4.4.4; atmospheric data from Reimer (2020).

patterned bone breakage, or the stacking of the bone assemblage described below.

Main Bone Assemblage

The main bone assemblage was derived mostly (95%) from the adult skeleton (**Figures 1–3** and **Supplementary Videos 1–10**). It included 44 broken cranial fragments, an intact upper right second molar (**Supplementary Video 7**) and 12 isolated tooth plates, 25 ribs broken into 52 fragments, 3 vertebrae and 15 vertebral fragments, 32 percussion-impact bone flakes, 9 'butterfly fragments' (below), 20 unidentifiable bone fragments, and 267 bags (6 × 10 cm and 10 × 17 cm) of small 'bone scraps' (below). Only two refits were found (**Supplementary Video 1**). The adult's face (tusks, premaxillae, and partial maxillae) is the single largest, heaviest element present and was positioned on top of the bone pile. It was sheared from the cranium at the nares, and its maxillary alveoli are broken and empty. The calf is represented by a partial left maxilla and dentary with intact dentitions (**Supplementary Figure 2**), three isolated tooth plates, left tibia diaphysis, and 10 rib fragments. This bone concentration occupied an area ∼1.5 m × ∼1.5 m; its excavated thickness, from the exposed tusk tip, is 1.1 m. It included numerous locally

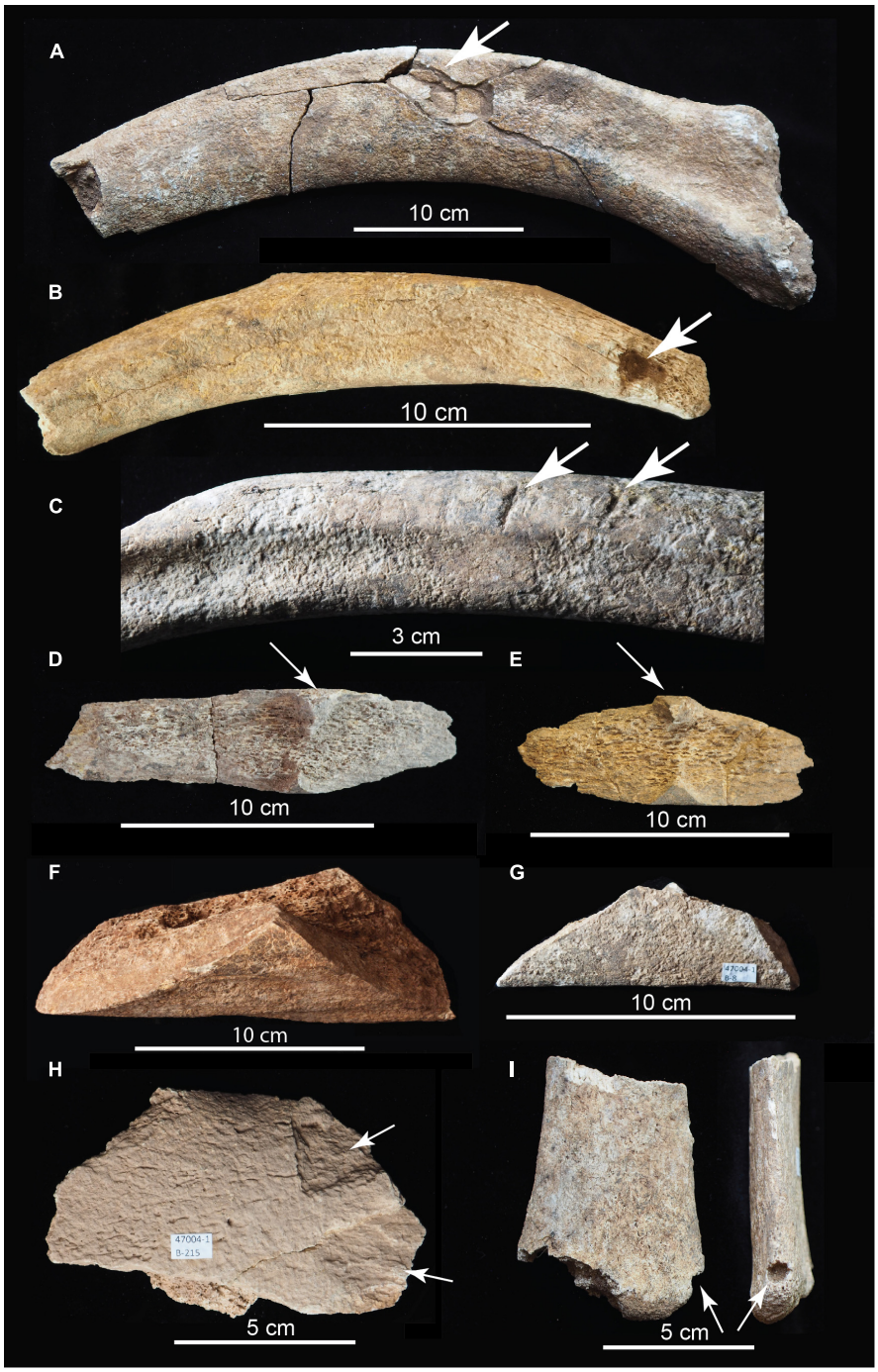

FIGURE 6 | Photographs of modified bones of adult Hartley mammoth. **(A)** Anterior rib with depressed blunt force impact wound (TMM 47004-1.1). **(B)** Mid-thoracic rib showing large-gauge puncture wound to capitulum (TMM 47004-1.36). **(C)** Mid-thoracic rib with parallel chop marks (TMM 47004-1.37). **(D,E)** Rib butterfly fragments (TMM 47004-1.152 and 47004-1.201). **(F)** Butterfly fragment derived from ulna or tibia (TMM 47004-1.40). **(G)** Rib butterfly fragment (TMM 47004-1.8). **(H)** Dentary bone flake with two secondary flake scars (TMM 47004-1.215). **(I)** Distal rib in two views showing puncture in-filled with sediment (TMM 47004-1.163) (**Supplementary Video 9**).

derived rounded sandstone cobbles weighing up to 3 kg. In the midst of the pile, lying on top of four broken ribs, was a 23.7 kg boulder interpreted as a hammerstone and/or anvil (**Figures 1**, **2**). The long axes of rib fragments and elongate bone fragments ($n = 40$) were mapped from photogrammetry images (**Figures 2A,B**) and subjected to Rao's spacing test ($p > 0.1$), Kuiper's test ($p > 0.15$), Rayleigh's test ($p = 0.927$), and Watson's test ($p > 0$). In each test, they failed to falsify the hypothesis

TABLE 2 | Quantitative amino acid analyses on Hartley adult mammoth bone collagen.

	Residues per thousand (R/1000)		
Amino acid	**HCl-decalcified collagen**	**EDTA-decalcified collagen**	**Sigma bovine collagen[1]**
Hydroxyproline	49	49	90
Aspartic acid	49	48	47
Threonine	20	20	17
Serine	37	36	31
Glutamic acid	85	83	73
Proline	136	136	114
Glycine	324	330	338
Alanine	132	130	113
Valine	26	26	26
Methionine	3	3	7
Isoleucine	10	10	12
Leucine	24	24	26
Tyrosine	0	0	4
Phenylalanine	13	12	20
Hydroxylysine	5	7	16
Lysine	34	34	21
Histidine	1	1	4
Arginine	51	51	39
Total	1000	1000	998

Specimen SR-9067 (TMM-47004-1.40, FN B40, N208.741 E98.122) compared to Sigma Modern Bovine Collagen. [1]Amino acid values are, by convention, reported in Residues per thousand (R/1000), as in this table; they are discussed in text as percentages.

of uniformity in orientation relative to the catchment channel axis (**Figure 2C**).

Most (88%) of the larger (>5 cm) bones and bone fragments in the main accumulation were buried in the lower two-thirds of the excavation, more than 35 cm below the modern colluvial surface. Every bone displays perimortem damage, save the adult right stylohyoid (**Supplementary Video 10**), which lay near the excavation floor. Two adult vertebral epiphyses remained in articulation with each other but were separated from their parent centra. Presumably, they were held together by an intact joint capsule at time of burial, one of many indications that burial was rapid. Buried beneath the adult face were a partial right frontal with an attached fragment of the nasal, the right parietal dome (**Figure 7** and **Supplementary Video 6**), and smaller fragments of pneumatic cranial wall (diplöe) that collectively represent less than one-third of the complete adult cranium.

Separation of the adult face from the cranium was caused by the most profound skull fracture, followed by fragmentation of the cranial vault. Dorsal surfaces of the frontal and parietal preserve multiple depressed, blunt-force impact fractures (**Figure 7**). One fragment of frontal plus nasal is depressed 5 cm into the anterior endocranial cavity. *En echelon* fractures mark its dorsal surface. Its persistent connection to the rest of the frontal suggests that skin and/or periosteal membrane were intact at time of burial. Other blunt impact fractures penetrated into diplöe of the frontal and parietal; CT scans reveal corresponding breakage of internal trabecular struts. The broken right parietal also bears two *en echelon* blunt-force impact fields ∼10 cm in diameter, implying perimortem skull breakage from repeated impacts to its dorsal surface. Proboscidean skulls are commonly fragmented in archeological sites to gain access to the brain and other soft tissues (Agam and Barkai, 2016, 2018; Fisher, 2021).

The adult frontal, 23 postcranial elements, and a calf tibia preserve circular cross-section punctures ∼2 mm to ∼1 cm in diameter (**Figures 6**, **8**, **9** and **Supplementary Video 9**). Large-diameter punctures occur in a cluster on the dorsal surface of the frontal; CT scans reveal detached surficial bone fragments displaced up to 15 mm into the diplöe. Small-diameter punctures also perforate the dorsal surface of the frontal, and two penetrate the orbital wall, entering obliquely from above. The locations and 3D geometries of these punctures are entirely inconsistent with carnivore canine marks (**Supplementary Information**).

Eleven right and 14 left ribs were identified; proximal and distal ends all exhibited perimortem damage. Costal epiphyses were detached from all but one rib head; six isolated costal epiphyses were recovered. On every proximal rib fragment (n = 23), the capitulum is damaged, exposing medullary cavities to sediment infilling. Six proximal rib heads (26%) display circular punctures or gouges measuring ∼1 cm in diameter. Ten ribs (40%) have small-diameter isolated punctures near their heads and on their shafts. Fifteen ribs (60%) preserve blunt-force impact fractures, and seventeen rib shafts (68%) are spirally fractured, indicating they were fresh when fractured. Short, broad, parallel chopmarks on one rib are consistent with expedient tools (Blasco et al., 2013; Rosell et al., 2014; Hannus, 2018). This damage suggests systematic rib detachment from the vertebral column, costal cartilages, sternum, and from

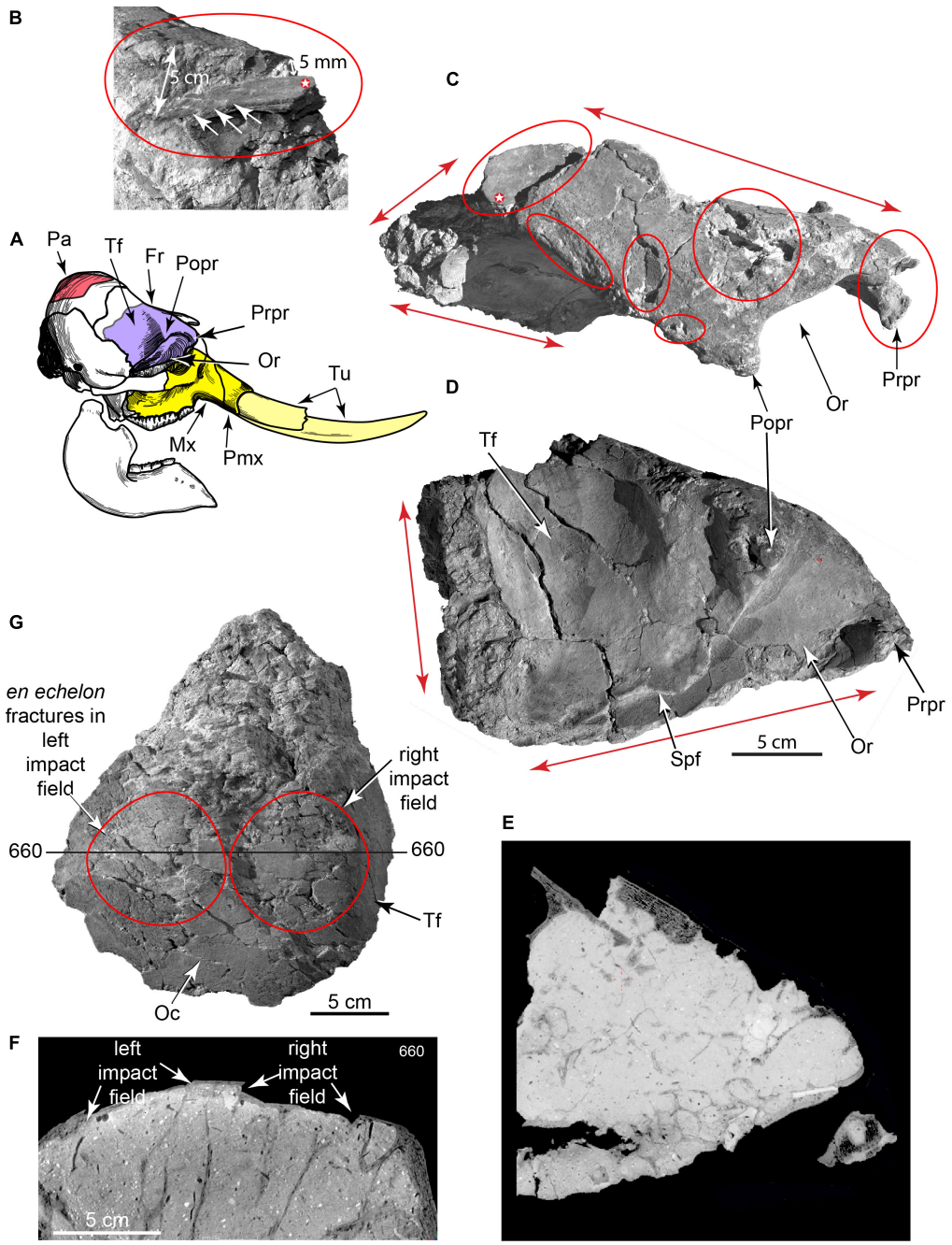

FIGURE 7 | 3D CT volumetric models and cross-sections of broken adult right frontal and right parietal. **(A)** Key to skull elements. **(B–D)** Partial right frontal in **(B)**, caudal **(C)**, dorsal and lateral views **(D)**, showing major fracture planes (red arrows F1, F2, F3, F4) where it was sheared from cranium (TMM 47004-1.31; **Supplementary Video 6**). Blunt-force impact wounds (Bfw 1, Bfw 2, Bfw 3), puncture wound concentrations (P1, P2), and two small-gauge punctures into orbital wall from obliquely above (P3, P4). **(E)** CT slice through frontal showing cemented grains in puncture channel P3 (red arrows), and offset bone from blunt force impact (Bfw 1). **(F)** CT slice through parietal showing impact-depressed bone (white arrows) and broken underlying trabeculae. **(G)** Broken right parietal dome showing right and left impact fields on dorsal surface (TMM 47004-1.213). Fr, frontal; Mx, maxilla; Oc, occipital surface of parietal; Or, orbit; Pa, parietal; Pmx, premaxilla; Popr, postorbital process; Prpr, preorbital process; Spf, sphenorbital fissure; Tf, temporal fossa; Tu, tusks.

each other using cylindrical rods and expedient cutting and chopping tools. Similar highly patterned carcass processing sequences have been described that may vary among taxa, but are largely standardized within a given taxon, and trace into the Old World Lower Paleolithic (Blasco et al., 2013; Rosell et al., 2014).

The three adult vertebral centra are missing their epiphyses; five separated centrum epiphyses were recovered. CT scans

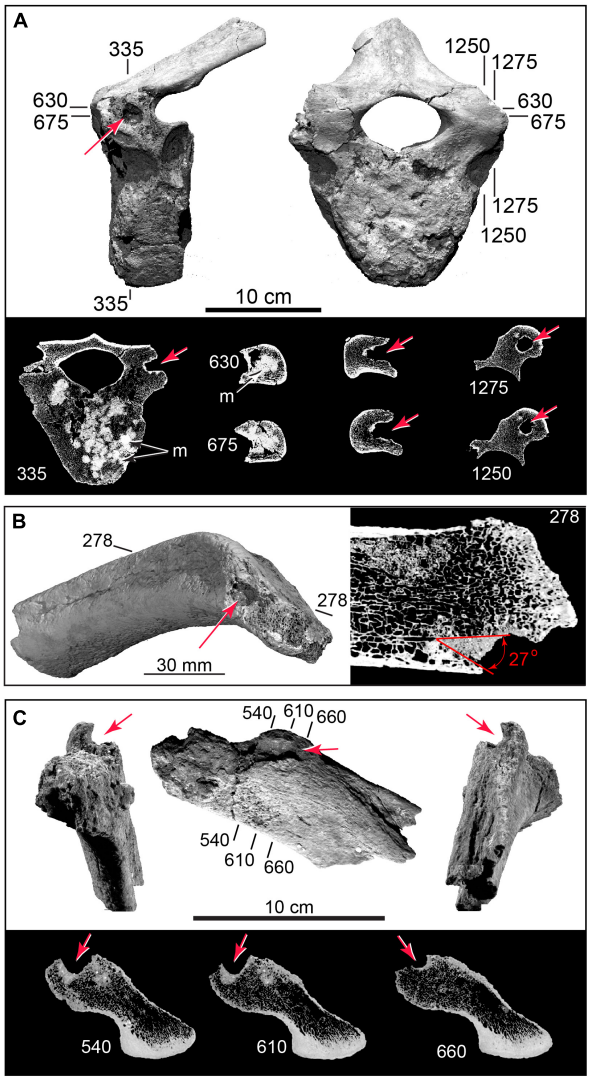

FIGURE 8 | 3D CT volumetric models and cross-sections of cylindrical punctures and cryptic punctures in vertebra and rib. **(A)** Thoracic vertebra with deep puncture in left transverse process; CT slices (below) showing puncture geometry in cross-section; and puncture cluster infilled by dense (bright) sediment (TMM 47004-1.22). **(B)** Puncture in rib head (TMM 47004-1.36). **(C)** Rib head (TMM 47004-1.2), with large-diameter (~10 mm) cylindrical gouge, and CT cross sections. Numbers refer to slice planes in CT datasets.

revealed 'cryptic' punctures in the centra not readily visible to the naked eye owing to postmortem sediment infillings whose color matches the bone. These include clusters of overlapping large-diameter punctures in all three centra, and penetrations extending up to 45 mm into the transverse processes (**Figure 8** and **Supplementary Video 8**). Following disarticulation of the vertebral column, the centra were separated from their epiphyses and repeatedly punctured, probably to facilitate grease extraction (Outram, 2001; Blasco et al., 2013; Fladerer et al., 2014; Rosell et al., 2014; Hannus, 2018; Fisher, 2021).

The adult appendicular skeleton is represented mostly by broken fragments, bone flakes, and 'butterfly fragments' (below). The left scapula is represented by a detached metacromion process, which is itself viewed as diagnostic of butchering as it provides a handle to carry the large muscle (*m. infraspinatus*) that attaches to it (Fisher, 2021). One complete carpal, two associated sesamoids, and two isolated phalanges were identified. The phalanges exhibit numerous small-diameter perimortem punctures that subsequently filled with sediment. Whereas carnivore canine penetrations are widest externally, tapering internally to a point, CT scans show these punctures are narrowest externally and broaden into wider chambers, suggesting insertion and rotation of a pointed tool that disrupted trabeculae, facilitating extraction of grease from cancellous bone interiors. The punctures probably occurred in conjunction with efforts to disarticulate grease-rich podial elements (Fisher, 1995) and retrieve pedal fat pads.

Bone Flakes

A significant feature of the Hartley site is the high number (n = 32) of bone flakes (**Figure 9**, **Supplementary Figure 3**, and **Supplementary Videos 1–5**); we restrict the term 'flake' to bone fragments preserving technical attributes associated with percussive forces (Fisher, 1995). Critics argue that, because scavenging and weathering can also reduce bones, bone flakes are not always culturally diagnostic (Meltzer, 2009; Waters et al., 2018; Waters, 2019). However, those from the Hartley locality preserve extraordinary patterning that geological processes or scavenging cannot explain. Most of the bone flakes (n = 22; 69%) were derived from thick cortical bone of the limbs, but cannot be assigned to a specific parent element with certainty; seven (22%) are from ribs; and three (9%) are from a dentary. Fifteen of the flakes (47%) have sharp edges suitable for cutting.

A remarkable pattern in these flakes is their consistent orientation with respect to the grain of their parent bone. The grain is the general trend of the cortical Haversian canal system and parent bone long-axis, and it controls fracture behavior in percussion events (Hannus, 1989, 2018; Bradfield, 2013; Shipman, 2018). Eleven (34%) flakes were struck parallel to the grain, 16 (50%) were struck perpendicular to the grain, and only five (16%) were of uncertain strike direction. In all, 78% (n = 25) of the bone flakes were struck either perpendicular or parallel to the grain of their parent bone. Such thorough, systematic attention to grain during bone reduction is unknown in non-cultural bone assemblages, including scavenged assemblages (e.g., Behrensmeyer et al., 1989).

Another remarkable pattern is that many bone flakes bear one or more secondary impact scars exhibiting preferential orientations to the grain of their parent flake. From a total of 50 secondary flake scars, 35 (70%) were struck parallel to the grain, 7 (14%) perpendicular, and eight (16%) were indeterminate as to strike direction. In all, 84% of the secondary scars were struck either perpendicular or parallel to the grain of their parent flakes. A chi-square test of bone flake strike and secondary flake scar directions returned a p-value of 0.001212 (the result is significant at $p < 0.05$). This indicates statistically significant patterned, systematic bone selection and reduction organized around grain and percussion-fracture behavior.

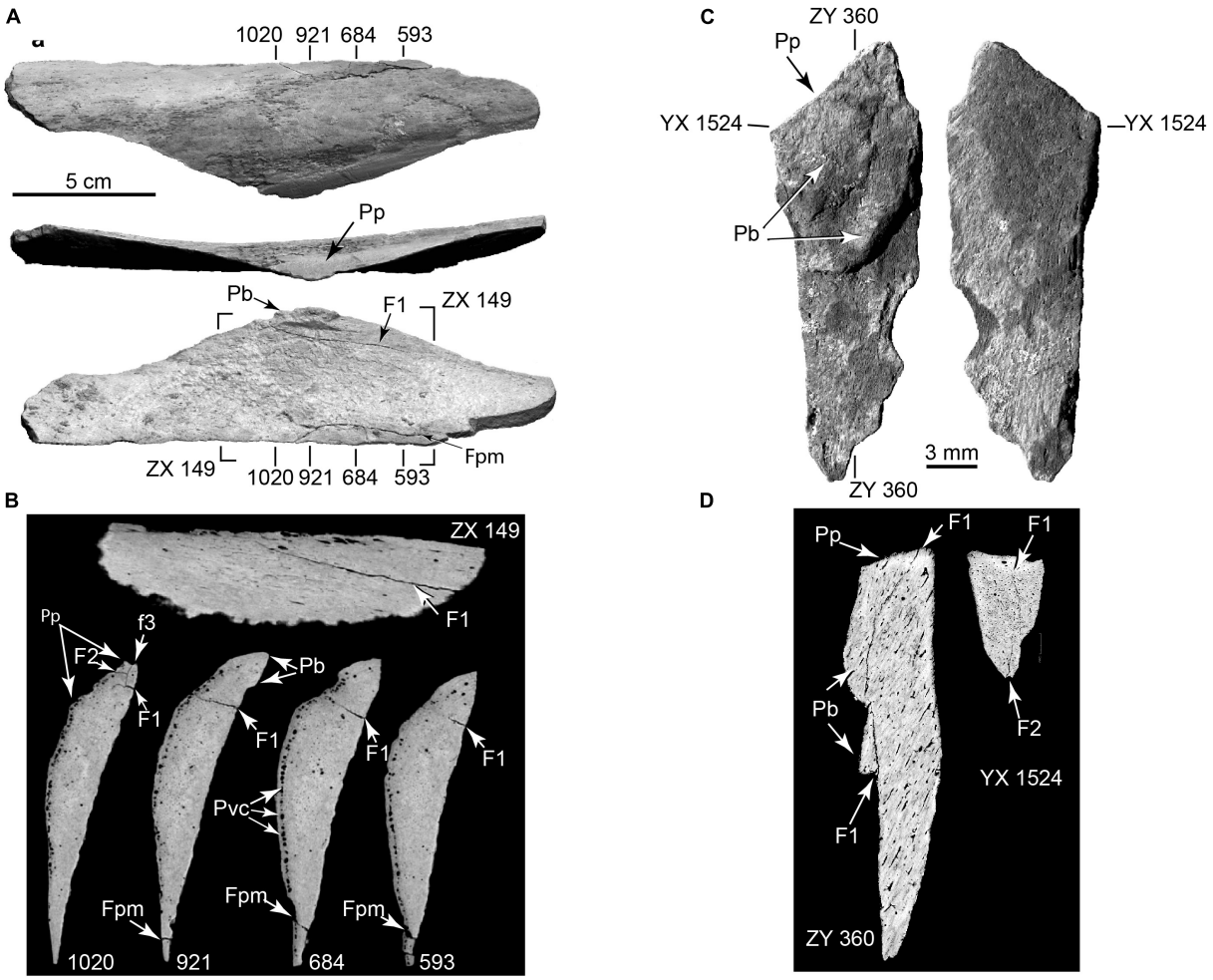

FIGURE 9 | Arrested fractures in bone flake and microflake. **(A)** Bone flake derived from limb diaphysis in external view (top), percussion surface view (middle), and internal view (bottom). **(B)** CT slices (numbered) showing arrested fractures (F1, F2, F3) propagating from percussion platform, and postmortem sediment loading fracture (fpm) (TMM 47004-1.70; **Supplementary Video 4**). **(C)** Opposite surfaces of microflake (TMM 47004-3.5.3a: **Supplementary Video 5**). **(D)** μCT slices showing arrested fractures (F1, F2). Pb, bulb of percussion; Pp, percussion platform; Pvc, periosteal vascular canals.

Following lithic terminology (Collins, 1999), we recognize bone 'microflakes' (**Figure 9**) that are less than 3 cm maximum length and exhibit some combination of the diagnostic features of larger flakes. The Hartley site actually preserved a continuum in flakes sizes but the term 'microflake' draws attention to the potential taphonomic importance of small bone fragments that are commonly overlooked (Outram, 2001).

Butterfly Fragments

Another important type of bone fragment, discussed in medical literature, is the "butterfly fragment" (Winquist and Hansen, 1980; Reber and Simmons, 2015; Cohen et al., 2016). Like bone flakes, butterfly fragments result from blunt force impact. Unlike bone flakes, which preserve technical attributes associated with percussive forces and compressive failure, butterfly fragments are products of tensile failure. They result from medium to high velocity impact to a limb diaphysis or rib and, if bending loads are sufficient, induce tensile failure that can spall butterfly fragments from the impact side of the diaphysis, the side opposite the impact, or both (**Supplementary Figure 4**). We recovered five butterfly fragments derived from limb elements and four from ribs. Butterfly fragments are always produced by blows perpendicular to the grain of the parent bone. Three of the butterfly fragments derived from limb diaphyses bear secondary flake scars struck parallel to the grain of the parent fragment. With rare exceptions (**Supplementary Information**), only humans are known to establish conditions in which limbs and ribs can break under tensile failure, producing these highly characteristic fragments. Sixteen of the bone flakes plus butterfly fragments (n = 41, 39%) preserve use-wear indicative of utilization as expedient tools (**Supplementary Information**). Similar bone flakes from other proboscidean butcher sites are described with compelling justification for interpreting them as percussion-flaked artifacts (Hannus, 1989, 2018; Fisher et al., 1994; Johnson, 2005; Pobiner et al., 2008;

Collins et al., 2013; Holen and Holen, 2013; Agam and Barkai, 2016; Holen et al., 2017; Fisher, 2021).

Arrested Fractures

To further enhance our understanding of bone flake formation and diagnosis, we CT scanned a manually knapped flake and microflake from fresh bovine bone, to document resulting fracture patterns (**Supplementary Figure 5**). As background, medical studies document healthy living bones containing "microcracks" that span distances of a few tens of micrometers. Typically, they are single features arising from *in vivo* mechanical stress not produced by point-loading, and may be stimuli for normal bone remodeling (Buckwalter et al., 1995; Poundarik and Vashishth, 2015). μCT shows fresh bone placed under static loads (trampling, scavenging, hide penetration) fails in relatively simple fractures that can extend for millimeters or centimeters, depending on load magnitude and bone size (Hannus, 1989, 2018; Shipman, 2018). However, under dynamic percussion-impact point-loading, where both force and loading rates are sufficiently high, CT revealed that a "fracture network" can propagate instantaneously into bone from the impact point, but only one or a few of the fractures rupture and separate flakes from parent bone. If all fractures in a network continued to the point of complete separation, the result would be a larger number of loose fragments, and CT scans of the entire assemblage would show no evidence of the process that generated them. CT reveals that this is not what happens. Simultaneous propagation of fractures in a network resulting from a single impact depends on the entire stress field generated by the impact. As soon as one of these fractures "breaks through," separating the original mass into two components, the stress field dissipates, preventing further propagation of remaining fractures in the network. Their further development is thus *arrested*, and precisely for this reason, they are retained in conjunction with the through-going fracture separating parent bone and flake. Using CT and μCT, we observed arrested fractures radiating from the impact point in a manually knapped modern bovine flake and microflake (**Supplementary Figure 5**), in flakes and a microflake from the Hartley assemblage (**Figure 9** and **Supplementary Videos 1–5**), and in three flakes from the Riley mammoth (University of Michigan UM 116967), which represents a very different taphonomic setting (Fisher, 2021). We recognize that the impact energy required to produce arrested fractures in bovine bone would be lower than that required for large mammoth diaphyses, but the comparability of arrested fractures in Hartley and Riley specimens, and arrested fractures in bovine bone, suggest that arrested fractures are indicative of much higher impact energies than simple fractures.

"Bone Scraps"

Dry-screening (3.175 mm mesh) all excavated matrix yielded a multitude of small (<3 cm) "bone scraps" that were derived from cranial diplöe and postcranial medullary bone. Similar "bone scrap" concentrations are reported in European sites (Outram, 2001; Fladerer et al., 2014). Hydrologic processes operating at the site fail to account for this extreme degree of fragmentation. However, crushing and boiling medullary bone is a common practice in grease procurement that produces such "bone scraps" as primary debris (Quigg, 1997; Costamagno et al., 2010; Fladerer et al., 2014; Hannus, 2018). While crushing may not increase the grease volume harvested, it increases efficiency because the smaller fragments require less water and fire (Marquer et al., 2010; **Supplementary Material**).

PYROGENIC PARTICLE ANALYSIS

Wet-screened (0.5 mm mesh) matrix samples from different vertical levels within the main bone accumulation yielded a diverse assemblage of micro-particles that are not eroded constituents of the escarpment supplying clastic particles to the colluvium. Microscopic examination of particles excavated from Old World hearths, in concert with combustion experiments, identified diagnostic residues of controlled fires fueled by burning wood, plant material, and bone (Bellomo, 1993; Schiegl et al., 1996; Alperson-Afil, 2008; Miller et al., 2010; Weiner, 2010; Aldeias et al., 2012; Aldeias, 2017). These particles include siliceous aggregates, subspherical complex aggregates of recrystallized ash, pulverized bone fragments, angular shattered tooth and bone fragments, vitrified plant fragments, and charcoal fragments.

Siliceous and Complex Aggregates

Siliceous aggregates are composites primarily of opal and quartz grains cemented by microcrystalline calcite into water insoluble, sub-spherical particles ranging in diameter from ∼1 to ∼8 mm (**Figure 10**). Such particles are well-known from excavations of Old World hearths, and their resistance to disaggregation aids in diagnosing the presence of fire (Schiegl et al., 1996). Siliceous aggregates form following the complete combustion of wood into calcium carbonate ash and opal phytoliths, as the pyrolyzed residue undergoes a series of diagenetic changes (Schiegl et al., 1996). Experiments indicate that formation of siliceous aggregates begins as wood is burned at combustion temperatures between 500 and 600°C, where calcium oxalate (CaC_2O_4) present in wood and bark is reduced to calcium carbonate ($CaC0_3$) as carbon monoxide (CO) burns off (Munro et al., 2007; Weiner, 2010). At still higher temperatures, between 700 and 850°C, the calcium carbonate is reduced to calcium oxide (CaO). Calcium oxide is generally unstable, and upon cooling, it reacts with atmospheric carbon dioxide (CO_2) to form secondary microcrystalline calcite, which becomes the primary binding agent of the siliceous aggregates. Alternatively, if the heated calcium oxide encounters water, it crystallizes to form calcium hydroxide or lime mortar [Ca_4 $(OH)_2$] (Weiner, 2010). Siliceous aggregates were recovered in abundance from wet-sieved matrix collected from within the main bone assemblage (**Figures 10A–D,I–K**). ESEM analysis detected trace amounts, in descending order of weight percentage, of aluminum, iron, magnesium, sodium, potassium, and sulfur. Some of the siliceous aggregates recovered from the Hartley site also contain bone fragment inclusions (**Figures 10E–K** and **Supplementary Videos 11, 12**).

Another class of abundant water-insoluble particles recovered from the sieved concentrate consists of "complex aggregates"

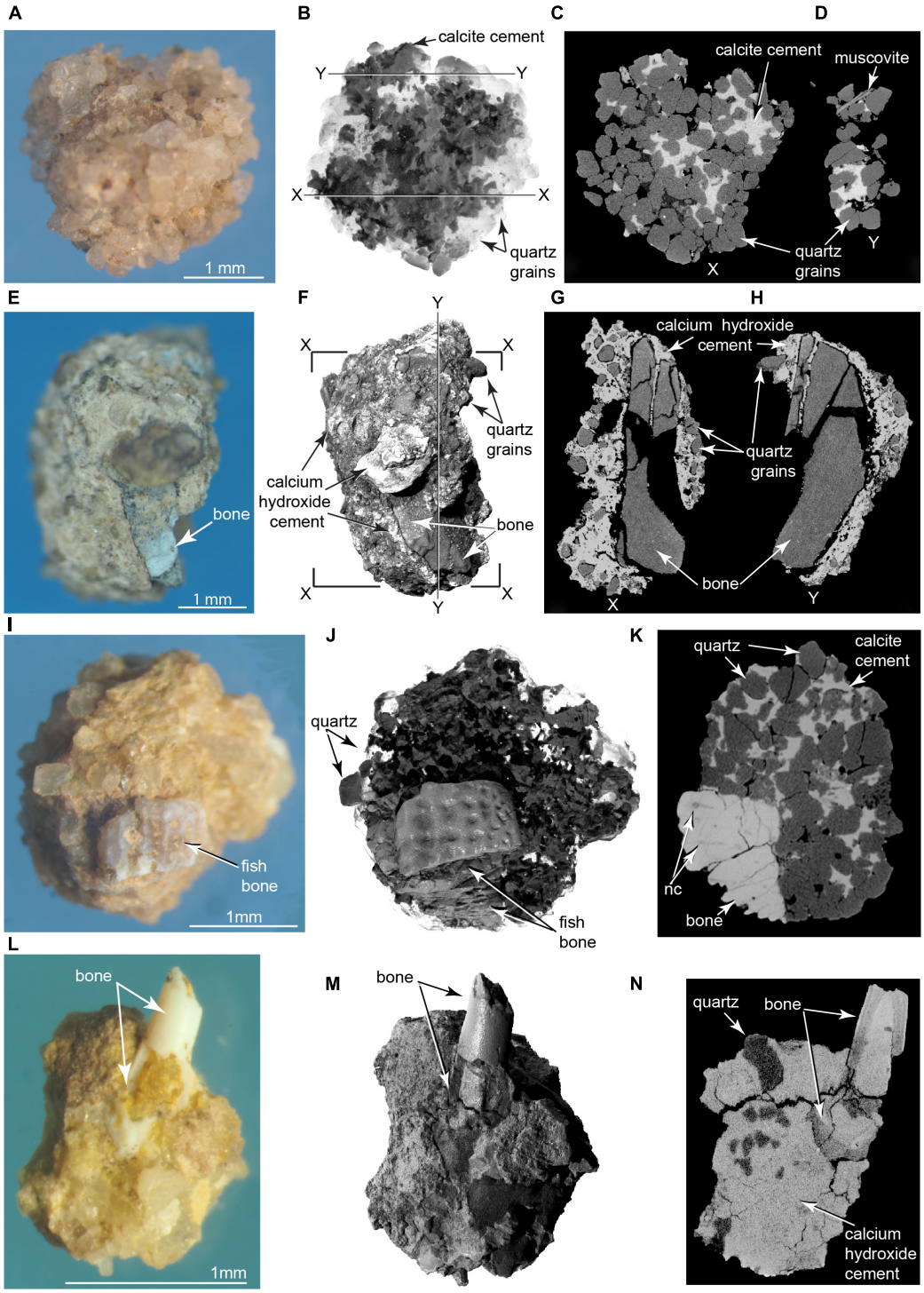

FIGURE 10 | Photomicrographs and μCT imagery of pyrogenic microparticles. Siliceous aggregate in **(A)** photomicrograph, **(B)** volumetric 3D reconstruction from μCT; **(C,D)** selected μCT slices in planes X and Y. Calcite (darker material) identified using ESEM in **(B)**, and as lighter material in **(C,D)** (TMM 47004-3.11.8). **(E–H)** Complex aggregate enclosing calcined bone fragment. **(E)** Photomicrograph, **(F)** μCT volumetric 3D reconstruction **(G,H)** μCT slices across aggregate containing pulverized bone fragment. Note in **(G,H)** penetration of ash into fractured bone, indicating degassing, shrinkage, and fracture of the bone were penecontemporaneous with calcium hydroxide crystallization (TMM 47004-3.12.1). **(I–K)** Ornamented fish cranial element cemented into siliceous aggregate in **(I)** photomicrograph, **(J)** volumetric 3D reconstruction from μCT, and **(K)** CT slice showing cementation of fish bone into the aggregate (**Supplementary Videos 9, 10**). nc, nerve canal in fish bone (TMM 47004-3.5.31). **(L–N)** Hollow fish radiale incorporated into complex aggregate of quartz grains cemented by microcrystalline calcium hydroxide matrix (identified using ESEM). **(L)** Photomicrograph, **(M)** volumetric 3D reconstruction from μCT; **(N)** μCT slice showing laminated histology of imbedded bone (TMM 47004-3.5.25).

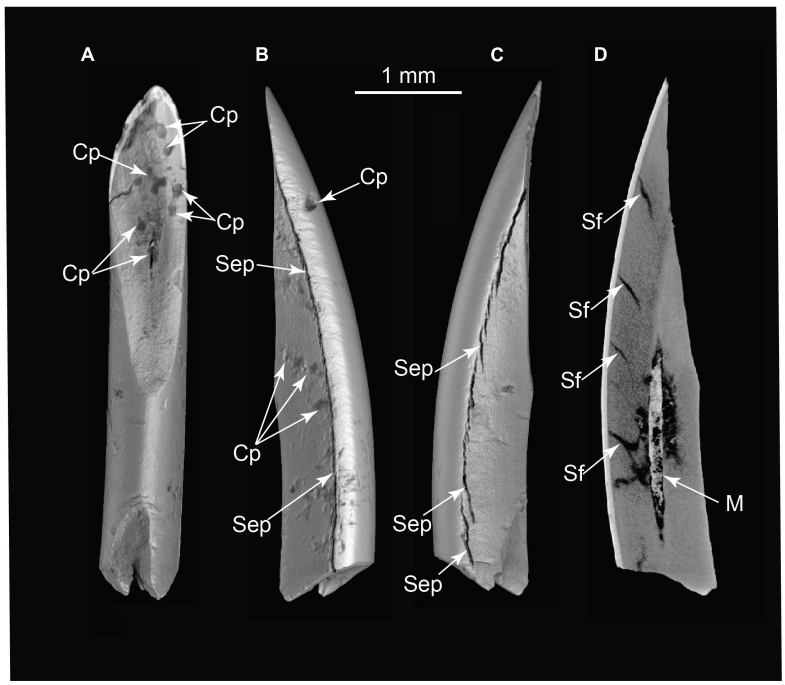

FIGURE 11 | Pyrogenic modifications to rodent incisor (volumetric reconstructions from μCT). **(A)** Occlusal view; **(B)** medial or lateral view; and **(C)** medial or lateral view; **(D)** CT slice revealing separation fractures and infilling of pulp cavity by ash. Cp, combustion pits; M, matrix in pulp cavity; Sep, separation by differential shrinkage at enamel-dentin junction; Sf, dentin shrinkage fractures in cross-section (TMM 47004-3.6.1b).

(Courty et al., 2012; Courty, 2017) that also range in size from ∼1 mm to ∼ 8 mm. ESEM analyses indicated their main component is microcrystalline calcite and lime mortar, which, together with iron oxide, cement together clastic grains of quartz, calcite, muscovite, feldspar, and other minerals derived from the Poleo Sandstone and Salitral Shale. Small fragments of bone are incorporated into a number of these aggregates (**Figures 10L–N**). ESEM analysis shows some bone inclusions to be calcined, indicating they were burnt. μCT scans reveal ash intruded into fractures in some of the bone fragments. ESEM and μCT analyses of ash-encrusted bone fragments (**Figures 10E–H**) suggest that degassing of water from green bone fragments induced hot calcium oxide to crystalize into insoluble lime mortar.

Pulverized Bone Fragments

Pulverized bone fragments as small as 1 mm are also abundant and display a spectrum of colors from tan to brown, red, light purple, to the pure white of calcined bone. Combustion experiments indicate that burning green bone produces the smallest fragments in the largest quantities, as physiological fluids contained in osteocyte lacunae, canaliculi, and vascular canals vaporize when heated, causing fresh bone and teeth to explode (Costamagno et al., 2010; Marquer et al., 2010). Bone is a common fuel in archeological fires, and pulverized bone and tooth fragments are virtually ubiquitous in pyrogenic residues excavated from Old World archeological hearths (Costamagno et al., 2010; Marquer et al., 2010; Fladerer et al., 2014). Calcination commences at ∼550–600°C (Hannus, 2018), and the presence of lime mortar in some aggregates indicates they were heated to temperatures exceeding 700°C (Weiner, 2010).

Vertebrate Microfauna

Vertebrate microfauna recovered from the wet-screened concentrate comprises an assemblage of angular fragments of teeth, fish scales, and rare intact disarticulated bones (**Figures 11**, **12** and **Supplementary Figure 7**). The fish scales are remarkable, considering the site is ∼70 m above the nearest river. μCT scans show traits diagnostic of burning, including circular combustion pitting and internal fractures from differential shrinkage of bone, dentin, and enamel (Hanson and Cain, 2007; Costamagno et al., 2010; Hannus, 2018). Fish scales and calcined bone were also found cemented into both siliceous aggregates and microaggregates (**Figure 10** and **Supplementary Videos 11, 12**), with an adhering insoluble rind of microcrystalline calcite and lime mortar not previously reported in association with microvertebrate fossils. This indicates these tiny bones are not contaminants from packrat middens or raptor roosts. Most microfaunal specimens are unidentifiable to the level of species or genus, but they hint at a greater cryptic biodiversity in the economy of this locality.

Similar assemblages of pyrolyzed particles are common in archaeological fires (Schiegl et al., 1996; Hanson and Cain, 2007; Costamagno et al., 2010; Marquer et al., 2010; Courty et al., 2012; Fladerer et al., 2014; Courty, 2017). They are not reported in wildfires, where faunal concentration mechanisms are unknown, and where wind, run-off, and pedogenic processes prevent

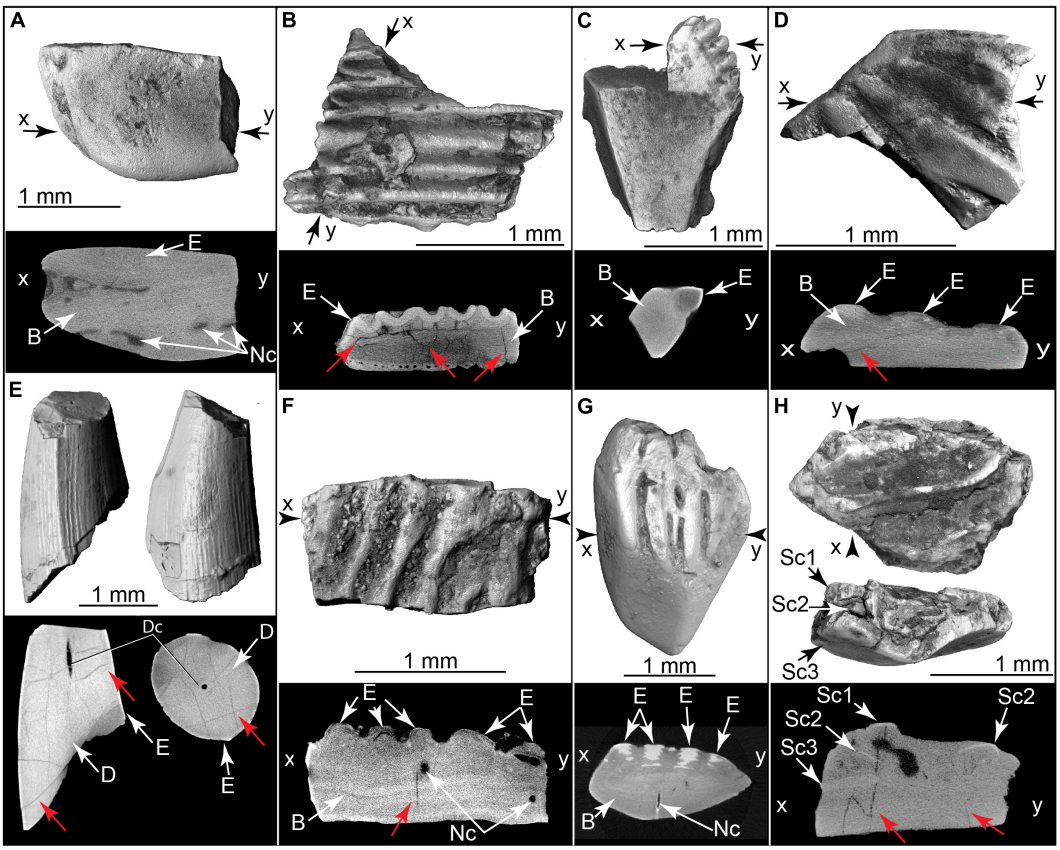

FIGURE 12 | Burnt fish teeth, fish bones, and fish scales. Volumetric 3D reconstructions from μCT (above) and histological cross section (below). Red arrows indicate internal heat fractures. **(A)** Gar scale and μCT cross section (TMM 47004-3.5.22c). **(B)** Cranial bone with enameloid covering, and μCT cross section (TMM 47004-3.5.17a). **(C)** Fin spine (Ictaluridae?) with enamel covering and μCT cross section (TMM 47004-3.11.10a). **(D)** Teleost scale and μ CT cross section (TMM 47004-3.12.5a). **(E)** Broken tooth in two views, plus μCT slices (below) in sagittal (left) and horizontal (right) planes (TMM 47004-3.12.5e). **(F)** Broken teleost scale and μ CT cross section (TMM 47004-3.11.10g). **(G)** Teleost scale and μCT cross section (TMM 47004-3.11.10f). **(H)** Imbricating burnt teleost scales and μCT cross section (TMM 47004-3.11.10c). B, bone; D, dentin; Dc, dental canal; E, enamel or enameloid; Nc, nerve canal; Sc1, scale 1; Sc2, scale 2; Sc3, scale 3.

the protected accumulation of ash and formation of siliceous and complex aggregates. At the Hartley site, the concentrated biodiversity and different burning states of pulverized bone, fish scales and teeth, and mammal teeth also argue against natural wildfire (Costamagno et al., 2010; Rosell et al., 2014; Agam and Barkai, 2016). This assemblage is not characteristic of flash heating by lightning, where much higher temperatures (∼1800°C) profoundly alter local mineralogy and offer no mechanism for faunal concentration (Essene and Fisher, 1986; Courty, 2017). In summary, this assemblage most likely formed in a controlled fire associated with the mammoth butchering.

LITHIC EVIDENCE

Lithic evidence consisted of six microflakes of Pedernal chert collected from levels between 40 and 65 cm deep into the matrix surrounding the main bone assemblage. μCT revealed diagnostic evidence of percussion flaking including prepared, ground percussion surfaces, bulbs of percussion, eraillure scarring, secondary flake scars with conchoidal separation surfaces, and hinge fractures (**Figure 13** and **Supplementary Video 13**). μCT scans also revealed arrested fractures in four of the lithic microflakes. Since surfaces can accumulate objects over time, and burrowing can mix sediment, it is conceivable that excavated chert microflakes are more recent surface contaminants. However, they were not found associated with burrows, and the fact that six were present favors their valid association with the mammoth bones.

DATING THE HARTLEY MAMMOTH LOCALITY

From a single adult long bone butterfly fragment (**Figure 6F**), six radiocarbon measurements were made on different bone collagen chemical fractions, including hydroxyproline (**Table 1** and **Figures 4**, **5**). Based on the hydroxyproline ^{14}C measurement, the adult mammoth dates to 32,750 ± 430 RCYBP (OxA-X-2737-65), with a calibrated date range of 38,900 – 36,250 cal BP. The five other AMS dates are in close agreement with each other and range from 30,860 + 220 to 28,100 + 350

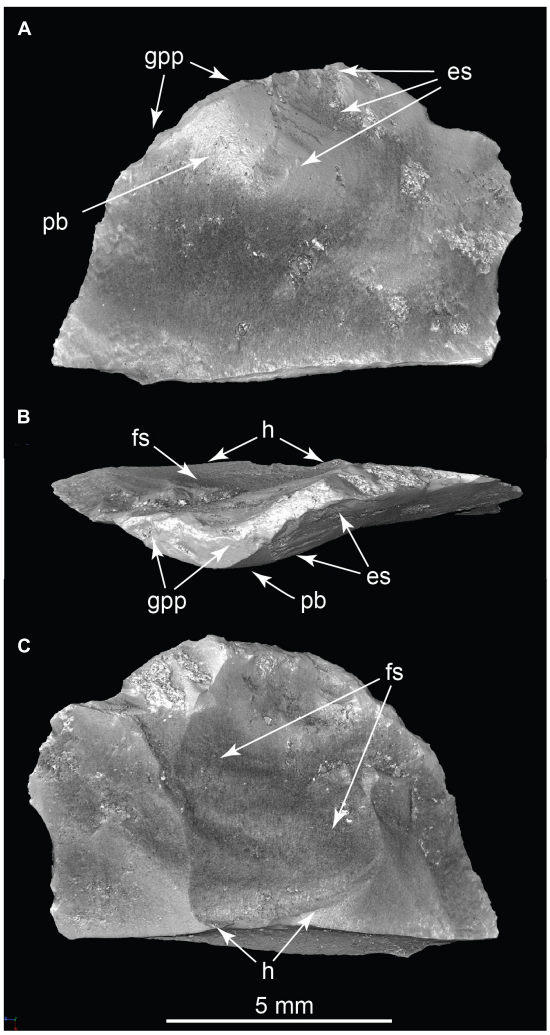

FIGURE 13 | Chert microflake in three views. **(A)** Internal aspect; **(B)** Striking platform; **(C)** External aspect. Es, eraillure scar on bulb of percussion; Fs, secondary flake scar showing ripple marks; H, secondary flake scar hinge; Pb, bulb of percussion; Gpp, ground percussion platform. (TMM 47004-5.1; **Supplementary Video 13**).

RCYBP (35,750 – 31,300 cal BP); however, the hydroxyproline measurement is oldest. Because the hydroxyproline "non-routine chemistry" protocol (see section "Methods") is considered the most efficient procedure for removing exogenous carbon from bone collagen samples, 32,750 + 430 RCYBP (38,900 – 36,250 cal BP) is the most robust age estimate for the adult mammoth.

DISCUSSION

The methods employed here are important for archeology generally as they can detect nuanced diagnostic evidence of human presence in unexpected geographic and temporal settings, and in the absence of stylized worked lithics. Pitulko et al. (2016a,b, 2017) used CT and bone breakage patterns to diagnose butchering of *Mammuthus primigenius* 45,000 years ago in the central Siberian Arctic locality of Sopochnaya Karga (see also Kenady et al., 2011). We augment and extend their findings by highlighting the diagnostic importance of butterfly fragments, and by demonstrating the application of CT and μCT in detecting arrested fracture networks in bone flakes and microflakes, particulate residues diagnostic of managed fires, and in documenting microfauna.

Our interpretation of the Hartley locality as a cultural site is consistent with other recent archeological discoveries placing humans in the Americas during or before the Last Glacial Maximum (LGM). These include multiple *in situ* human footprints from New Mexico that date from ∼22,860 to ∼21,130 cal BP (Bennett et al., 2021), and footprints from Argentina that date to ∼30,000 cal BP (Azcuy et al., 2021). Simple stone tools discovered in Chiquihuite Cave, Mexico, date from ∼26,500 to 19,000 cal BP and represent a previously unknown tradition (Ardelean et al., 2020; Becerra-Valdivia and Higham, 2020). At Coxcatlan Cave, Mexico, re-dating butchered small mammals associated with minimally worked stone tools established a 33,448 to 28,279 cal BP date for the site's lowest cultural level (Somerville et al., 2021). Simple flaked stone artifacts are known from numerous ancient South American sites. These include Toca da Tira Peia, Brazil, which dates to ∼20,000 cal BP (Lahaye et al., 2013), and Vale da Pedra Furada, Brazil, which dates to ∼24,000 cal BP (Boëda et al., 2021); older artifacts dating to ∼32,000 cal BP are also reported from this site (Guidon and Delibrias, 1986; Guidon et al., 1994). At Toca do Serrote das Moendas, Brazil, faunal remains associated with human bones were dated to between ∼29,000 and ∼24,000 cal BP (Kinoshita et al., 2014). And at Arroyo del Vizcaíno, Uruguay, a fossil-rich 30,000 years old megafaunal locality with cut-marked bones (Fariña et al., 2014) adds to a growing record of probable human occupation sites in the Americas that predate arrival of the Native American clade by millennia.

One method to test the hypothesis of an early human occupation in the Americas is to compare it against a broader context or system of independent generalizations (Ghiselin, 1969), such as genomic research on human populations using aDNA. These studies corroborate our findings and permit inferences regarding distinct cultural elements of the different migrations. This resolves nagging anomalies in archeological records, presents a far deeper time frame for attainment by humans of a global distribution (with the exception of Antarctica and most oceanic islands), and a longer time span for human roles in extinctions and ecological change across the Western Hemisphere.

Recent genomic evidence for two Old World founding populations in the Americas (Skoglund et al., 2015) offers independent corroboration that the sites described above may be cultural. A unique ancestry signal discovered in Suruí, Karitiana, and Xavante populations living today around the Amazon basin rim was found to be shared with living populations in Australia, New Guinea, and Andaman Islands. The ancestral population that contributed this signal was termed a "genetic ghost population" and given the name "Population Y" (Skoglund et al., 2015). Population Y was estimated to have occupied eastern Asia ∼50,000 years ago (Reich, 2018). Additional aDNA support

came from a ∼40,000 years old human bone from Tianyuan cave in northern China that shares the Population Y signal (Yang et al., 2017). Doubts raised about the Population Y hypothesis (Posth et al., 2018) were dispelled by more recent genomic studies that reproduced the earlier findings and documented in South America the Australasian signal in every major linguistic group, making it geographically widespread (Castro et al., 2021).

How and when Population Y ancestry reached South America has been explained by alternative hypotheses (Skoglund et al., 2015; Reich, 2018). The first is that Population Y contributed ancestry to the Native American clade before its dispersal south from Beringia. Some of the Native Americans then carried this ancestry as they dispersed down the west coast and into South America. In other words, Population Y predated dispersal but did not live in the Americas, and its descendants now solely exist there and in Australasia (Wohns et al., 2022). This has been the favored hypothesis because it is consistent with the conventional view that Native Americans were the first people to enter the Americas ∼16,000 years ago.

However, several recent aDNA analyses that included a ∼45,000 years old human genome from Ust'-Ishim, Siberia (Fu et al., 2014), ∼32,000 years old human genomes from the Yana RHS site (Sikora et al., 2019), and younger ancient Asian genomes (Poznik et al., 2016), revealed complex patterns of dispersal, admixture, and turnover among West Eurasian and East Asian populations in the occupation of Siberia and western Beringia. Marine Isotope Stage 3 (MIS 3, ca. 50,000 – 30,000 cal BP) was evidently a time of rapid expansion of modern humans across Eurasia (Atkinson et al., 2008; Poznik et al., 2016; Pavlova and Pitulko, 2020), but no Population Y ancestry was detected by any of these studies (Sikora et al., 2019).

The second hypothesis is that unmixed descendants of Population Y dispersed directly to the Americas during pre-LGM time, predating the Native American arrival by millennia (Skoglund et al., 2015; Reich, 2018). This early population was later displaced by the Native Americans except in South America, where it mixed with Native Americans and left a discernable signal in every major living linguistic group. This now seems the more likely, because the first hypothesis alone fails to explain archeological sites that predate Native American arrival.

At present, the oldest human aDNA in the Americas is from the Anzick child burial site that includes diagnostic Clovis artifacts and dates to 12,905 – 12,695 cal BP (Becerra-Valdivia et al., 2018). aDNA places this individual on the stem of the Native American clade (Rasmussen et al., 2014); it preserves no Population Y ancestry. The absence of a Population Y signal in North America may be an artifact of the lack of human bones and aDNA older than ∼13,000 cal BP, and under-sampling of living populations. Until much older human aDNA is recovered, uncertainty will attend the association of Population Y with any of the older archeological sites. It is technically possible that the older American sites represent entirely separate, unrecognized pre-LGM lineage(s) that became extinct without leaving a discernable genetic trace in younger populations (Raff, 2022).

It is not surprising that the cultural interpretation of these "old" sites received criticism (Chatters et al., 2021; Potter et al., 2021). Implicit in the criticisms is an expectation that diagnostic Upper Paleolithic stone tools are the standard by which all American cultural sites are recognized. However, if Native Americans were the first to introduce this technology into the Americas ∼16,000 years ago, such evidence should not be present in older sites. Raff (2022) observed that "probably most" American archeologists maintain a need to uniformly apply a rigorous standard for accepting any and all sites. The fallacy of such a view is that evidentiary standards and rationales may have temporal and geographic boundaries. For example, the 33,000 cal BP site of Monte Verde I, located near the southern tip of Chile, preserved simple worked-stone implements and proboscidean bones in association with clay-lined hearth basins (Dillehay and Collins, 1988). Few archeologists have been willing to recognize this seemingly anomalous site as cultural. However, viewed in light of the older Hartley site and its location on the North American Colorado Plateau, Monte Verde I no longer presents an anomaly in time or space. Given their ages, the absence of elaborate stone tools is to be expected at both localities. Another example of spatiotemporal evidentiary limits is the meticulous re-dating of the North America Clovis interval to a narrow window of only ∼200 calendar years, between 13,125 and 12,925 cal BP (Waters and Stafford, 2007; Becerra-Valdivia et al., 2018; Waters et al., 2020). It follows that any cultural sites in the Americas predating arrival by Native Americans will necessarily be diagnosed using criteria other than Upper Paleolithic stone tools.

In summary, taphonomic and genomic evidence accord in detecting at least two founding populations for the Americas, and in viewing the story of Native Americans expanding into virgin country as "profoundly misleading" (Reich, 2018). The position of the Hartley site deep in the North American Western Interior suggests that the first human arrival in North America, whether overland or via a coastal route, occurred well before ∼37,000 years ago. The Hartley site shares much in common with Old World proboscidean butchering sites; it appears that while hunting technologies evolved steadily, butchering practices preserved more stable procedural efficiencies. The Hartley locality exemplifies new methods and nuanced criteria for diagnosing early human occupation sites in the archeological record. It raises provocative new questions about when, where, and how the Native American clade, with its unprecedented technology, intersected with earlier human occupants of the Americas. It also provides a new deep point of chronologic reference for occupation of the Americas, for attainment by humans of a global distribution, and a temporal recalibration of human ecological impacts across the Western Hemisphere.

DATA AVAILABILITY STATEMENT

The datasets presented in this study can be found in online repositories. The names of the repository/repositories and accession number(s) can be found below: all excavated specimens and samples are curated into the collections of the University of Texas Vertebrate Paleontology Laboratory. All CT datasets are archived at UTCT (http://www.ctlab.geo.utexas.edu/) and are available on reasonable request.

AUTHOR CONTRIBUTIONS

TR coordinated the field work, preparation and curation of fossils, wrote the manuscript, and processed the images. TS conducted the ^{14}C dating, assisted the field interpretation, and wrote the manuscript. DF wrote the manuscript and produced the experimental bone flakes. JE performed the proteomic analysis and edited the manuscript. RH conducted the ESEM analyses and edited the manuscript. JQ studied bone modifications, microflakes and wrote the manuscript. JS identified and curated the microfauna. RK edited the manuscript, conducted the statistical analyses, and analyzed the CT data. MC edited the manuscript and conducted the CT scanning and data archiving. All authors contributed to the article and approved the submitted version.

FUNDING

Funding was provided by the Jackson School of Geosciences, and by National Science Foundation grants BCS 1541294, EAR 1258878, EAR-1160721, EAR 1919700, EAR 1561622, and EAR 1762458, and the W. J. J. Gordon Foundation.

ACKNOWLEDGMENTS

We thank K. Bader, J. Biorkmann, B. A. S. Bhullar, E. Catlos, R. Cifelli, M. Collins, M. Cloos, G. N. Hartley, T. Higham, E. Hoffman, S. Holen, B. Huckell, H. Hutchison, C. Jass, J. Kappelman, C. Kerans, J. Koser, T. Liebert, E. Lundelius, L. MacFadden, C. Merriam, G. Meyer, D. Mohrig, J. Muus, R. Probiner, J. Singh, J. Stevens, J. Sturm, W. Taylor, L. Becerra-Valdivia, and M. W. Young for contributions to this report.

SUPPLEMENTARY MATERIAL

The Supplementary Material for this article can be found online at: https://www.frontiersin.org/articles/10.3389/fevo.2022.903795/full#supplementary-material

REFERENCES

Agam, A., and Barkai, R. (2016). Not the brain alone: the nutritional potential of elephant heads in Paleolithic sites. *Quat. Int.* 406, 218–226.

Agam, A., and Barkai, R. (2018). Elephant and mammoth hunting during the Paleolithic: a review of the relevant archaeological, ethnographic and ethno-historical records. *Quaternary* 1, 1–28. doi: 10.3390/quat1010003

Aldeias, V. (2017). Experimental approaches to archaeological fire features and their behavioral relevance. *Curr. Anthropol.* 58, S191–205.

Aldeias, V., Goldberg, P., Sandgathe, D., Berna, F., Dibble, H. L., and McPherron, S. P. (2012). Evidence for Neandertal use of fire at Roc de Marsal (France). *J. Archaeol. Sci.* 39, 2414–2423.

Alperson-Afil, N. (2008). Continual fire-making by hominins at Gesher Benot Ya'aqov, Israel. *Quat. Sci. Rev.* 27, 1733–1739.

Ardelean, C. F., Becerra-Valdivia, L., Pedersen, M. W., Schwenninger, J. L., and Oviatt, C. G. (2020). Evidence of human occupation in Mexico around the Last Glacial Maximum. *Nature* 584, 87–92. doi: 10.1038/s41586-020-2509-0

Atkinson, Q. D., Gray, R. D., and Drummond, A. J. (2008). mtDNA variation predicts population size in humans and reveals a major Southern Asian chapter in human prehistory. *Mol. Biol. Evol.* 25, 468–474. doi: 10.1093/molbev/msm277

Azcuy, C. L., Carrizo, H. L., Tonni, E. P., Panarello, H. O., and Rodriguez, A. (2021). Late Pleistocene fossil hominid tracks on the beaches of Claromecó, Argentina. *Acta Geol. Lilloana* 33, 43–57.

Bar-Yosef, O. (2002). The upper paleolithic revolution. *Ann. Rev. Anthropol.* 31, 363–393. doi: 10.3389/fpsyg.2012.00569

Becerra-Valdivia, L., and Higham, T. (2020). The timing and effect of the earliest human arrivals in North America. *Nature* 584, 93–97. doi: 10.1038/s41586-020-2491-6

Becerra-Valdivia, L., Waters, M. R., Stafford, T. W. Jr., Anzick, S. L., Comeskey, D., Devièse, T., et al. (2018). Reassessing the chronology of the archaeological site of Anzick. *Proc. Natl. Acad. Sci. U. S. A.* 115, 7000–7003. doi: 10.1073/pnas.1803624115

Behrensmeyer, A. K., Gordon, K. D., and Yanagi, G. T. (1989). "Nonhuman bone modification in Miocene fossils from Pakistan," in *Bone Modification*, eds R. Bonnichsen and M. Sorg (Orono: Center for the Study of the First Americans), 99–120.

Behrensmeyer, A. K., and Hill, A. P. (1988). *Fossils in the Making: Vertebrate Taphonomy and Paleoecology*. Chicago, IL: University of Chicago Press.

Bellomo, R. V. A. (1993). Methodological approach for identifying archaeological evidence of fire resulting from human activities. *J. Archaeol. Sci.* 20, 525–553.

Bennett, M. R., Bustos, D., Pigati, J. S., Springer, K. B., Urban, T. M., Holliday, V. T., et al. (2021). Evidence of humans in North America during the Last Glacial Maximum. *Science* 373, 1528–1531.

Blasco, R., Rosell, J., Domínguez-Rodrigo, M., Lozano, S., Pastó, I., Riba, D., et al. (2013). Learning by heart: cultural patterns in the faunal processing sequence during the Middle Pleistocene. *PLoS One* 8:e55863. doi: 10.1371/journal.pone.0055863

Boëda, E., Ramos, M., Pérez, A., Hatté, C., Lahaye, C., Pino, M., et al. (2021). 24.0 kyr cal BP stone artefact from Vale da Pedra Furada, Piauí, Brazil: techno-functional analysis. *PLoS One* 16:e0247965. doi: 10.1371/journal.pone.0247965

Bradfield, J. (2013). Investigating the potential of micro-focus computed tomography in the study of ancient bone tool function: results from actualistic experiments. *J. Archaeol. Sci.* 40, 2606–2613.

Brock, F., Higham, T., Ditchfield, P., and Ramsey, C. B. (2010). Current pretreatment methods for AMS radiocarbon dating at the Oxford radiocarbon accelerator unit (ORAU). *Radiocarbon* 52, 103–112.

Buckwalter, J. A., Glimcher, M. J., Cooper, R. R., and Recker, R. (1995). Bone biology. Part I: structure, blood supply, cells, matrix, and mineralization. *J. Bone Joint Surg. Br.* 77, 1256–1275. doi: 10.1002/jbmr.3394

Carlson, W. D., Rowe, T., Ketcham, R. A., Colbert, M. W., et al. (2003). "Geological Applications of High-Resolution X-ray Computed Tomography in Petrology," in *Meteoritics and Palaeontology. In: Applications of X-ray Computed Tomography in the Geosciences*, eds F. Mees, R. Swennen, M. Van Geet, and P. Jacobs (London: Geological Society of London), 7–22.

Castro, M. A., Ferraz, T., Bortolini, M. C., Comas, D., and Hünemeier, T. (2021). Deep genetic affinity between coastal Pacific and Amazonian natives evidenced by Australasian ancestry. *Proc. Natl. Acad. Sci. U. S. A.* 118, e2025739118. doi: 10.1073/pnas.2025739118

Chatters, J. C., Potter, B. A., Prentiss, A. M., Fiedel, S. J., and Haynes, G. (2021). Evaluating Claims of Early Human Occupation at Chiquihuite Cave, Mexico. *PaleoAmerica* 8, 1–16.

Cohen, H., Kugel, C., May, H., Medlej, B., Stein, D., Slon, V., et al. (2016). The impact velocity and bone fracture pattern: forensic perspective. *Forensic Sci. Int.* 266, 54–62. doi: 10.1016/j.forsciint.2016.04.035

Collins, M. (1999). *Clovis Blade Technology*. Austin, TX: University of Texas Press.

Collins, M. B., Stanford, D., Lowery, D., and Bradley, B. (2013). "North America before Clovis: variance in temporal/spatial cultural patterns, 27,000–13,000 cal yr BP," in *Paleoamerican Odyssey*, eds K. E. Graf, C. V. Ketron, and M. R. Waters (College Station, TX: Texas A & M University Press), 521–539.

Costamagno, S., Théry-Parisot, I., Kuntz, D., Bon, F., and Mensan, R. (2010). Taphonomic impact of prolonged combustion on bones used as fuel,

the taphonomy of burned organic residues and combustion features in archaeological contexts. *Palethnologie* 2, 169–183.

Courty, M. A. (2017). Fuel origin and firing product preservation in archaeological occupation contexts. *Quat. Int.* 431, 116–130.

Courty, M. A., Carbonell, E., Poch, J. V., and Banerjee, R. (2012). Microstratigraphic and multi-analytical evidence for advanced Neanderthal pyrotechnology at Abric Romani (Capellades, Spain). *Quat. Int.* 247, 294–312.

Devièse, T., Karavanić, I., Comeskey, D., Kubiak, C., Korlević, P., Hajdinjak, M., et al. (2017). Direct dating of Neanderthal remains from the site of Vindija Cave and implications for the Middle to Upper Paleolithic transition. *Proc. Natl. Acad. Sci. U. S. A.* 114, 10606–10611. doi: 10.1073/pnas.1709235114

Devièse, T., Stafford, T. W. Jr., Waters, M. R., Wathen, C., Comeskey, D., Becerra-Valdivia, L., et al. (2018a). Increasing accuracy for the radiocarbon dating of sites occupied by the first Americans. *Quat. Sci. Rev.* 198, 171–180.

Devièse, T., Comeskey, D., McCullagh, J., Bronk Ramsey, C., and Higham, T. (2018b). New protocol for compound specific radiocarbon analysis of archaeological bones. *Rapid Commun. Mass Spectrom.* 32, 373–379. doi: 10.1002/rcm.8047

Dillehay, T. D., and Collins, M. B. (1988). Early cultural evidence from Monte Verde in Chile. *Nature* 332, 150–152.

Essene, E. J., and Fisher, D. C. (1986). Lightning strike fusion: extreme reduction and metal-silicate liquid immiscibility. *Science* 234, 189–194. doi: 10.1126/science.234.4773.189

Fariña, R. A., Tambusso, P. S., Varela, L., Czerwonogora, A., Di Giacomo, M., Musso, M., et al. (2014). Arroyo del Vizcaíno, Uruguay: a fossil-rich 30-ka-old megafaunal locality with cut-marked bones. *Proc. Biol. Sci.* 281:20132211. doi: 10.1098/rspb.2013.2211

Fisher, D. C. (2021). "Underwater carcass storage and processing of marrow, brains, and dental pulp: Evidence for the role of proboscideans in human subsistence," in *Human-Elephant Interactions: From Past to Present*, eds G. E. Konidaris, R. Barkai, V. Tourloukis, and K. Harvati (Tübingen: Tübingen University Press), 407–435.

Fisher, D. C., Lepper, B. T., and Hooge, P. E. (1994). "Evidence for butchery of the Burning Tree mastodon," in *The First Discovery of America: Archaeological Evidence of the Early Inhabitants of the Ohio Area*, ed. W. S. Dancy (Columbus: Ohio Archaeological Council), 43–57.

Fisher, J. W. (1995). Bone surface modifications in zooarchaeology. *J. Archaeol. Method Theory* 2, 7–68.

Fladerer, F. A., Salcher-Jedrasiak, T. A., and Händel, M. (2014). Hearth-side bone assemblages within the 27 ka BP Krems-Wachtberg settlement: fired ribs and the mammoth bone-grease hypothesis. *Quat. Int.* 351, 115–133.

Frank, L. R., Rowe, T. B., Boyer, D. M., Witmer, L. M., and Galinsky, V. L. (2021). Unveiling the Third Dimension: automated quantitative volumetric computational morphometry. *Sci. Rep.* 11:14438. doi: 10.1038/s41598-021-93490-4

Frison, G. C., and Todd, L. C. (1986). *Colby Mammoth Site: Taphonomy and Archaeology of a Clovis kill in Northern*. Wyoming: University of New Mexico Press.

Fu, Q., Li, H., Moorjani, P., Jay, F., Slepchenko, S. M., Bondarev, A. A., et al. (2014). Genome sequence of a 45,000-year-old modern human from western Siberia. *Nature* 514, 445–449. doi: 10.1038/nature13810

Ghiselin, M. (1969). *The Triumph of the Darwinian Method*. Berkeley, CA: University of California Press.

Guidon, N., and Delibrias, G. (1986). Carbon-14 dates point to man in the Americas 32,000 years ago. *Nature* 321, 769–771.

Guidon, N., Parenti, F., de Fatima Da Luz, M., Guérin, C., and Faure, M. (1994). Le plus ancien peuplement de l'Amérique: le Paléolithique du Nordeste brésilien. *Bull. Soc. Prehistorique Française* 91, 246–250.

Hannus, L. (1989). "A. Flaked mammoth bone from the Lange/Ferguson site, White River badlands area, South Dakota," in *Bone Modification*, eds R. Bonnichsen and M. Sorg (Orono: Center for the Study of the First Americans), 395–412.

Hannus, L. A. (ed.) (2018). *Clovis Mammoth Butchery: The Lange/Ferguson Site and Associated Bone Tool Technology*. College Station, TX: Texas A & M University Press.

Hanson, M., and Cain, C. (2007). Examining histology to identify burned bone. *J. Archaeol. Sci.* 34, 1902–1913.

Haynes, G., Krasinski, K., and Wojtal, P. (2020). Elephant bone breakage and surface marks made by trampling elephants: implications for interpretations of marked and broken *Mammuthus* spp. bones. *J. Archaeol. Sci. Rep.* 33:102491.

He, L., Diedrich, J., Chu, Y. Y., and Yates, J. R. (2015). Extracting accurate precursor information for tandem mass spectra by rawconverter. *Anal. Chem.* 87, 11361–11367. doi: 10.1021/acs.analchem.5b02721

Hedges, R. E. M., and van Klinken, G. J. (1992). A review of current approaches in the pretreatment of bone for radiocarbon dating by AMS. *Radiocarbon* 34, 279–291.

Holen, S. R., Deméré, T. A., Fisher, D. C., Fullagar, R., Paces, J. B., Jefferson, G. T., et al. (2017). A 130,000- year-old archaeological site in southern California, USA. *Nature* 544, 479–483. doi: 10.1038/nature22065

Holen, S. R., and Holen, K. A. (2013). "The mammoth steppe hypothesis: the middle Wisconsin (Oxygen Isotope Stage 3) peopling of North America," in *Paleoamerican Odyssey*, eds K. E. Graff, C. V. Ketron, and M. R. Waters (College Station, TX: Texas A & M University Press), 429–444.

Huckell, B., Rowe, T., McFadden, L., Meyer, G., and Merriman, C. (2016). "The hartley mammoth site, north-central New Mexico," *The 81st Annual Meeting of the Society for American Archaeology (Orlando, Florida)*, Orlando: Society for American Archaeology.

Johnson, E. (2005). "Late-Wisconsinan mammoth procurement in the North American grasslands," in *Paleoamerican Origins: Beyond Clovis*, ed. R. Bonnichsen (College Station, TX: Texas A & M University Press), 161–182.

Kenady, S. M., Wilson, M. C., Schalk, R. F., and Mierendorf, R. R. (2011). Late Pleistocene butchered *Bison antiquus* from Ayer Pond, Orcas Island, Pacific Northwest: age confirmation and taphonomy. *Quat. Int.* 233, 130–141.

Kinoshita, A., Skinner, A. R., Guidon, N., Ignacio, E., Felice, G. D., Buco, C. A., et al. (2014). Dating human occupation at Toca do Serrote das Moendas, São Raimundo Nonato, Piauí-Brasil by electron spin resonance and optically stimulated luminescence. *J. Human Evol.* 77, 187–195. doi: 10.1016/j.jhevol.2014.09.006

Kowalewski, M., Goodfriend, G. A., and Flessa, K. W. (1998). High-resolution estimates of temporal mixing within shell beds: the evils and virtues of time-averaging. *Paleobiology* 24, 287–304.

Lahaye, C., Hernandez, M., Boëda, E., Felice, G. D., and Guidon, N. (2013). Human occupation in South America by 20,000 BC: the Toca da Tira Peia site, Piauí, Brazil. *J. Archaeol. Sci.* 40, 2840–2847.

Marquer, L., Otto, T., Nespoulet, R., and Chiotti, L. (2010). A new approach to study the fuel used in hearths by hunter-gatherers at the Upper Palaeolithic site of Abri Pataud (Dordogne, France). *J. Archaeol. Sci.* 37, 2735–2746.

Meltzer, D. J. (2009). *First Peoples in a New World – Colonizing Ice Age America*. Berkeley, CA: University of California Press.

Meltzer, D. J. (2015). *The Great Paleolithic War*. Chicago, IL: University of Chicago Press.

Miller, C. E., Conard, N. J., Goldberg, P., and Berna, F. (2010). Dumping, sweeping and trampling: experimental micromorphological analysis of anthropogenically modified combustion features. *Palethnologie* 2, 25–37.

Munro, L. E., Longstaffe, F. J., and White, C. D. (2007). Burning and boiling of modern deer bone: effects on crystallinity and oxygen isotope composition of bioapatite phosphate. *Palaeogeogr. Palaeoclimatol.* 249, 90–102.

Outram, A. K. (2001). A new approach to identifying bone marrow and grease exploitation: why the "indeterminate" fragments should not be ignored. *J. Archaeol. Sci.* 28, 401–410.

Pavlova, E. Y., and Pitulko, V. V. (2020). Late Pleistocene and Early Holocene climate changes and human habitation in the arctic Western Beringia based on revision of palaeobotanical data. *Quat. Int.* 549, 5–25.

Pitulko, V., Pavlova, E., and Nikolskiy, P. (2017). Revising the archaeological record of the Upper Pleistocene Arctic Siberia: human dispersal and adaptations in MIS 3 and 2. *Quat. Sci. Rev.* 165, 127–148.

Pitulko, V. V., Tikhonov, A. N., Pavlova, E. Y., Nikolskiy, P. A., Kuper, K. E., and Polozov, R. N. (2016a). Early human presence in the Arctic: evidence from 45,000-year-old mammoth remains. *Science* 351, 260–263. doi: 10.1126/science.aad0554

Pitulko, V. V., Pavlova, E. Y., and Basilyan, A. E. (2016b). Mass accumulations of mammoth (mammoth 'graveyards') with indications of past human activity in the northern Yana-Indighirka lowland, Arctic Siberia. *Quat. Int.* 406, 202–217.

Pobiner, B. L., Rogers, M. J., Monahan, C. M., and Harris, J. W. (2008). New evidence for hominin carcass processing strategies at 1.5 Ma, Koobi Fora, Kenya. *J. Hum. Evol.* 55, 103–130. doi: 10.1016/j.jhevol.2008.02.001

Posth, C., Nakatsuka, N., Lazaridis, I., Skoglund, P., Mallick, S., Lamnidis, T. C., et al. (2018). Reconstructing the Deep Population History of Central and South America. *Cell* 175, 1185–1197. doi: 10.1016/j.cell.2018.10.027

Potter, B. A., Chatters, J., Prentiss, A. M., Fiedel, S. J., Haynes, G., Kelly, R. L., et al. (2021). Current understanding of the earliest human occupations in the Americas: evaluation of Becerra-Valdivia and Higham. *PaleoAmerica* 8, 62–76. doi: 10.1080/20555563.2021.1978721

Poundarik, A. A., and Vashishth, D. (2015). Multiscale imaging of bone microdamage. *Connect. Tissue Res.* 56, 87–98. doi: 10.3109/03008207.2015.1008133

Poznik, G. D., Xue, Y., Mendez, F. L., Willems, T. F., Massaia, A., Wilson Sayres, M. A., et al. (2016). Punctuated bursts in human male demography inferred from 1,244 worldwide Y-chromosome sequences. *Nat. Genet.* 48, 593–599. doi: 10.1038/ng.3559

Quigg, J. M. (1997). Bison processing at the Rush site, 41TG346, and evidence for pemmican production in the Southern Plains. *Plains Anthropol.* 42, 145–161.

Raff, J. (2022). *Origin: A Genetic History of the Americas*. New York, NY: Hatchette Book Group.

Raghavan, M., Skoglund, P., Graf, K., Metspalu, M., Albrechtsen, A., and Moltke, I. (2014). Upper Palaeolithic Siberian genome reveals dual ancestry of Native Americans. *Nature* 505, 87–91. doi: 10.1038/nature12736

Rappsilber, J., Mann, M., and Ishihama, Y. (2007). Protocol for micro-purification, enrichment, pre-fractionation and storage of peptides for proteomics using StageTips. *Nat. Protoc.* 2, 1896–1906. doi: 10.1038/nprot.2007.261

Rasmussen, M., Anzick, S. L., Waters, M. R., Skoglund, P., and DeGiorgio, M. (2014). The genome of a Late Pleistocene human from a Clovis burial site in western Montana. *Nature* 506, 225–229. doi: 10.1038/nature13025

Reber, S. L., and Simmons, T. (2015). Interpreting injury mechanisms of blunt force trauma from butterfly fracture formation. *J. Forensic Sci.* 60, 1401–1411. doi: 10.1111/1556-4029.12797

Reich, D. (2018). *Who We Are and How We Got Here: Ancient DNA and the New Science of the Human Past*. Oxford: Oxford University Press.

Reimer, P. J. (2020). Composition and consequences of the IntCal20 radiocarbon calibration curve. *Quat. Res.* 96, 22–27.

Rosell, J., Blasco, R., Peris, J. F., Carbonell, E., and Barkai, R. (2014). Recycling bones in the Middle Pleistocene: some reflections from Gran Dolina TD10-1 (Spain), Bolomor cave (Spain) and Qesem Cave (Israel). *Quat. Int.* 361, 297–312.

Rowe, T. B., and Frank, L. R. (2011). The vanishing third dimension. *Science* 331, 712–714.

Schiegl, S., Goldberg, P., Bar-Yosef, O., and Weiner, S. (1996). Ash Deposits in Hayonim and Kebara Caves, Israel: macroscopic, microscopic and mineralogical observations, and their archaeological implications. *J. Archaeol. Sci.* 23, 763–781.

Schwarcz, H. P., and Nahal, H. (2021). Theoretical and observed C/N ratios in human bone collagen. *J. Archaeol. Sci.* 131:105396.

Shipman, P. (1981). *Life History of a Fossil: An Introduction to Taphonomy and Paleoecology*. Cambridge, MA: Harvard University Press.

Shipman, P. A. (2018). "Scanning electron microscopy evaluation of the Lange/Ferguson mammoth bone assemblage: bone fracture, technology, and use-wear in taphonomic context," in *Clovis Mammoth Butchery: The Lange/Ferguson Site and Associated Bone Tool Technology*, ed. A. L. Hannus (College Station, TX: Texas A & M University Press), 117–136.

Sikora, M., Pitulko, V. V., Sousa, V. C., Allentoft, M. E., Vinner, L., Rasmussen, S., et al. (2019). The population history of northeastern Siberia since the Pleistocene. *Nature* 570, 182–188. doi: 10.1038/s41586-019-1279-z

Skoglund, P., Mallick, S., Bortolini, M., Chennagiri, N., Hünemeier, T., Petzl-Erler, M. L., et al. (2015). Genetic evidence for two founding populations of the Americas. *Nature* 525, 104–108. doi: 10.1038/nature14895

Somerville, A. D., Casar, I., and Arroyo-Cabrales, J. (2021). New AMS radiocarbon ages from the preceramic levels of coxcatlan Cave, Puebla, Mexico: a pleistocene occupation of the Tehuacan valley?. *Latin Am. Antiq.* 32, 1–15.

Stafford, T. W. Jr. (2014). "Chronology of the Kennewick Skeleton, Washington," in *The Scientific Investigation of an Ancient American Skeleton*, eds D. W. Owsley and R. L. Jantz (College Station, TX: Texas A & M University Press), 58–89.

Stafford, T. W. Jr., Hare, P. E., Currie, L., Jull, A. J. T., and Donahue, D. J. (1991). Accelerator radiocarbon dating at the molecular level. *J. Archaeol. Sci.* 18, 35–72.

Waters, M. R. (2019). Late Pleistocene exploration and settlement of the Americas by modern humans. *Science* 365:eaat5447. doi: 10.1126/science.aat5447

Waters, M. R., Keene, J. L., Forman, S. L., Prewitt, E. R., and Carlson, D. L. (2018). Pre-Clovis projectile points at the Debra L. Friedkin site, Texas—Implications for Late Pleistocene peopling of the Americas. *Sci. Adv.* 4:eaat4505. doi: 10.1126/sciadv.aat4505

Waters, M. R., Stafford, T. W. Jr., and Carlson, D. L. (2020). The age of Clovis – 13,050 to 12,750 cal yr B.P. *Sci. Adv.* 6:eaaz0455. doi: 10.1126/sciadv.aaz0455

Waters, M. R., Stafford, T. W. Jr., Kooyman, B., and Hills, L. V. (2014). Late Pleistocene horse and camel hunting at the southern margin of the ice-free corridor: reassessing the age of Wally's Beach, Canada. *Proc. Natl. Acad. Sci. U. S. A.* 112, 4263–4267. doi: 10.1073/pnas.1420650112

Waters, M. R., and Stafford, T. W. (2007). Redefining the age of Clovis: implications for the peopling of the Americas. *Science* 315, 1122–1126.

Weiner, S. (2010). *Microarchaeology: Beyond the Visible Archaeological Record*. Cambridge: Cambridge University Press.

Winquist, R. A., and Hansen, S. T. Jr. (1980). Comminuted fractures of the femoral shaft treated by intramedullary nailing. *Orthop. Clin. North Am.* 11, 633–648.

Wohns, A. W., Wong, Y., Jeffery, B., Akbari, A., Mallick, S., Pinhasi, R., et al. (2022). A unified genealogy of modern and ancient genomes. *Science* 375:eabi8264. doi: 10.1126/science.abi8264

Yang, M. A., Gao, X., Theunert, C., Tong, H., Aximu-Petri, A., Nickel, B., et al. (2017). 40,000-year-old individual from Asia provides insight into early population structure in Eurasia. *Curr. Biol.* 27, 3202–3208. doi: 10.1016/j.cub.2017.09.030

Conflict of Interest: TR declares that he owns the land on which the site was discovered. TS was employed by Stafford Research, LLC, Albuquerque, NM, United States.

The remaining authors declare that the research was conducted in the absence of any commercial or financial relationships that could be construed as a potential conflict of interest.

Publisher's Note: All claims expressed in this article are solely those of the authors and do not necessarily represent those of their affiliated organizations, or those of the publisher, the editors and the reviewers. Any product that may be evaluated in this article, or claim that may be made by its manufacturer, is not guaranteed or endorsed by the publisher.